Journal of Structural Geology 145 (2021) 104287

Contents lists available at ScienceDirect

Journal of Structural Geology

journal homepage: http://www.elsevier.com/locate/jsg

Active tectonics and kinematics of Fethiye-Göcek Bay, SW Turkey: Insight about the eastern edge of Pliny-Strabo Trenches

Levent Tosun [a,b], Ulaş Avşar [a], Özgür Avşar [c], Derman Dondurur [d], Nuretdin Kaymakcı [a,*]

[a] Department of Geological Engineering, Middle East Technical University, 06531 Ankara, Turkey
[b] Cardiff University, School of Earth and Ocean Sciences, 2.28, Main BuildingPark Place, Cardiff, Turkey
[c] Department of Geological Engineering, Muğla Sıtkı Koçman University, 48000, Muğla, Turkey
[d] Institute of Marine Sciences and Technology, Dokuz Eylül University, 35340, İzmir, Turkey

ARTICLE INFO

Keywords:
Pliny-strabo trench
Fethiye-burdur fault zone
Fethiye-göcek bay
Kinematic analysis
Seismic interpretation
Paleostress inversion

ABSTRACT

Pliny-Strabo Trench (PST)is a Subduction Transform Edge Propagator (STEP) fault developed at the northern edge of the African oceanic lithosphere connecting the Aegean and Cyprian trenches in the eastern Mediterranean. Recent studies have demonstrated that the PST terminates close to Turkish Border and links to the Cyprian trench east of Rhodes and south of Fethiye-Göcek Bay. However, it is also claimed that the PST extends into SW Anatolia along a sinistral transtensional shear zone, so-called Fethiye-Burdur Fault Zone (FBFZ) implying that a lithospheric tear in the downgoing plate extends into the over-riding plate, although, this is kinematically almost impossible since full mechanical coupling between down going and the over-riding plate is necessary. To test this hypothesis and understand the kinematics of the transition zone between PST and Cyprian trench we have conducted a rigorous paleostress inversion study combined with interpretation of 2D seismic data of which 228 km total length obtained from Fethiye-Göcek Bay.

The seismic reflection data are used for the interpretation and delineation of off-shore faults and to determine their recent activity. The geometry and kinematics of the exposed on-land faults are determined by analyzing 13969 fault slip data obtained from 211 sites distributed evenly throughout in an area encompassing the bay in an area extending 70 km in E-W and 50 km in N–S that cover the whole area where the Pliny-Strabo STEP fault would emerge on-land.

Results of analyses indicated that most of the faults in the study area are developed under multi-directional extension, except for some NE-SW-striking faults, which have dextral strike-slip components contrary to proposed sinistral nature of Fethiye-Burdur Fault Zone. Although there are numerous normal faults some which have been active until recently, however, there is almost no NE-SW striking sinistral strike-slip fault in the region to justify the presence of Fethiye-Burdur Shear Zone. Additionally, there are a number of earthquakes with dominantly strike-slip moment tensor solutions in the deeper part of the bay while they are in normal character in the on-shore areas suggesting that the Pliny-Strabo Trench stops very close to the shoreline and it does not propagate into SW Anatolia. Therefore, existence and alleged characteristics of the Fethiye-Burdur Fault Zone could not be verified.

1. Introduction

The present-day geological configuration and the recent evolution of the Western Anatolia have been shaped as a result of two continuing tectonic processes that include collision and northwards convergence of the Arabian Plate causing westward extrusion of the Anatolian Plate along the North Anatolian and East Anatolian Fault Zones (Şengör and Yilmaz, 1981) and the long-lasting northwards and still-active subduction of African lithosphere, which is segmented and retreating southwards along the Aegean and Cyprian trenches (McKenzie, 1978; Le Pichon and Angelier, 1979; Biryol et al., 2011) (Fig. 1). It is generally accepted that due to slab tearing resulted from the lateral variation in the mechanical properties of the subducted lithosphere, the Aegean and Cyprus trenches are segmented by about 100 km wide transform fault zone, called as Pliny-Strabo trench (Woodside et al., 2002; Govers and Wortel, 2005). After the recognition of this shear zone based on seismic

* Corresponding author.
E-mail address: kaymakci@metu.edu.tr (N. Kaymakcı).

https://doi.org/10.1016/j.jsg.2021.104287
Received 17 May 2020; Received in revised form 6 January 2021; Accepted 19 January 2021
Available online 26 January 2021

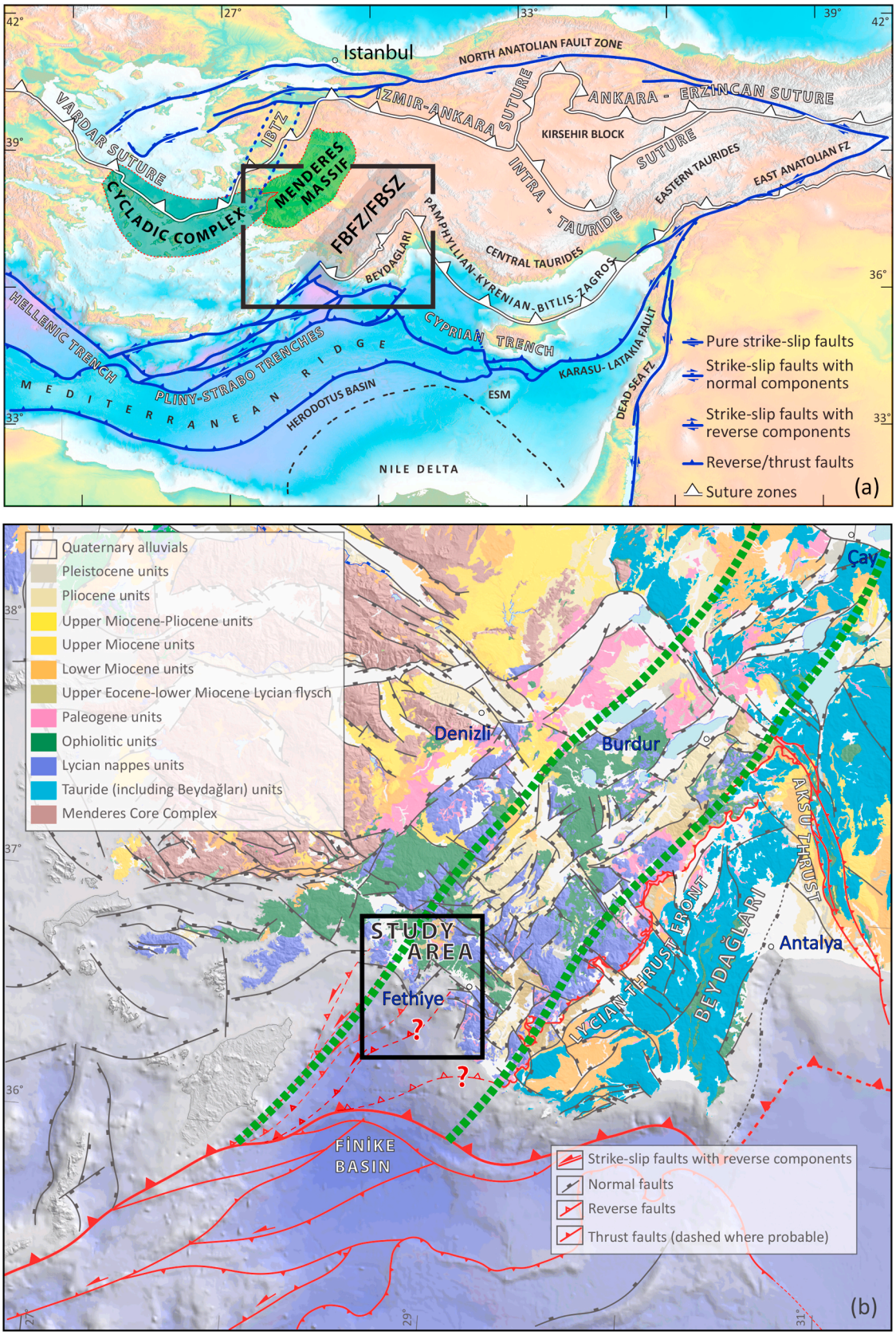

Fig. 1. a) Simplified tectonic scheme of the Eastern Mediterranean region (Kaymakci et al., 2009, 2018). ESM: Eratosthenes Seamount FBFZ/FBSZ: previously proposed position of Fethiye-Burdur Fault (Barka and Reilinger, 1997), (Shear) Zone (Hall et al., 2014). R: Rhodes Basin. Note that Pliny-Strabo Trench terminates at the northern end of Rhodes Basin. b) Simplified geological map of SW Anatolia and location of the study area (adapted from Kaymakcı et al., 2018; Özkaptan et al., 2018). Possible extension of Pliny-Strabo Trenches is based on Ocakoğlu (2012). The approximate position of Fethiye-Burdur Shear Zone of Hall et al. (2014) is illustrated with green dashed lines. (For interpretation of the references to color in this figure legend, the reader is referred to the Web version of this article.)

tomographic studies (van Hinsbergen et al., 2010; Biryol et al., 2011), it has been proposed that Pliny Strabo trench continues in the over-riding plate, on land SW Anatolia as a sinistral transtensional shear zone, the so-called Fethiye-Burdur Fault Zone (FBFZ), (Elitez, 2010; Tiryakioğlu et al., 2013; Hall et al., 2014).

In this context, the scope of this paper is documenting the active tectonics and kinematics characteristics of the Fethiye-Göcek Bay, which is located at the northern edge of the Pliny-Strabo trench where it may possibly extend further northwards into the on-land areas of SW Anatolia (Fig. 1) (Dumont et al., 1979; Barka and Reilinger, 1997; Ocakoğlu, 2012). For this purpose, we have used 13969 fault slip data collected from 221 locations and interpretation of seismic sections obtained from sparker seismic data acquisition from the Fethiye Bay.

The kinematic analysis, based on fault slip data sets, aims at unravelling the paleostress orientations and their relative magnitudes which provide information about the style and pattern of deformation in an area of investigation. Seismic data combined with bathymetric data provide detection of active faults which also help to map their geometry and spatial distribution.

The definition of an active fault is arbitrary, and it is designated based on the likelihood of occurrence of an earthquake on a fault that could affect the safety of engineering structures (Machette, 2000). However, in this study active fault is designated as the faults that cut and displaces the youngest deposits at the sea bottom. Therefore, the combination of paleostress analysis of faults on land and mapped faults on the sea bottom provides a complete data set for their activity and characteristics. This information is crucial for evaluating the connection between the Pliny-Strabo trenches and their possible northwards continuation as a sinistral strike-slip fault zone, at least during the Quaternary. Furthermore, this information allows us testing the hypothesis whether (i) there is a sinistral strike-slip fault zone in the study area that developed in response to northwards propagation of the Pliny-Strabo STEP fault on land and accommodate differential motion between Aegean and Central Anatolian regions, as proposed by Hall et al. (2014) or (ii) it terminates around the Fethiye-Göcek Bay, do not extend into the on land SW Anatolian region but they connect Hellenic and Cyprian trenches (Kaymakcı et al., 2018).

2. Geological setting

The SW Anatolia is one of the most extensively studied portions of Turkey due to its role in the geodynamic evolution of the Eastern Mediterranean as being located near the transition zone between Hellenic and Cyprian trenches. The pre-Neogene rock units in SW Turkey comprises three major tectonostratigraphic units. From west to east, they include the Menderes Massif, the Lycian Nappes, and the Bey Dağları Platform (Figs. 1 and 2). These units are separated by major structural contacts and constitute an entirely exposed section of products of subduction, obduction, collision, and post-orogenic core-complex development processes associated with the closure of Neotethys ocean (Şengör and Yilmaz, 1981).

The Menderes Massif represents a relatively autochthonous Pan-African basement as a gneissic metamorphic core complex (Bozkurt and Park, 1994) and is overlain by a pre-Eocene metasedimentary cover, which comprises a passive margin carbonate platform units of Mesozoic-Early Cenozoic age (Özgül 1984; Özer et al., 2001). The Lycian Nappes comprises ophiolites developed in a supra-subduction zone setting during the late Early Cretaceous (Collins and Robertson, 1997), and various Mesozoic carbonated sequences which collectively accreted and thrusted over the Menderes Massif and Beydağları Platform. These

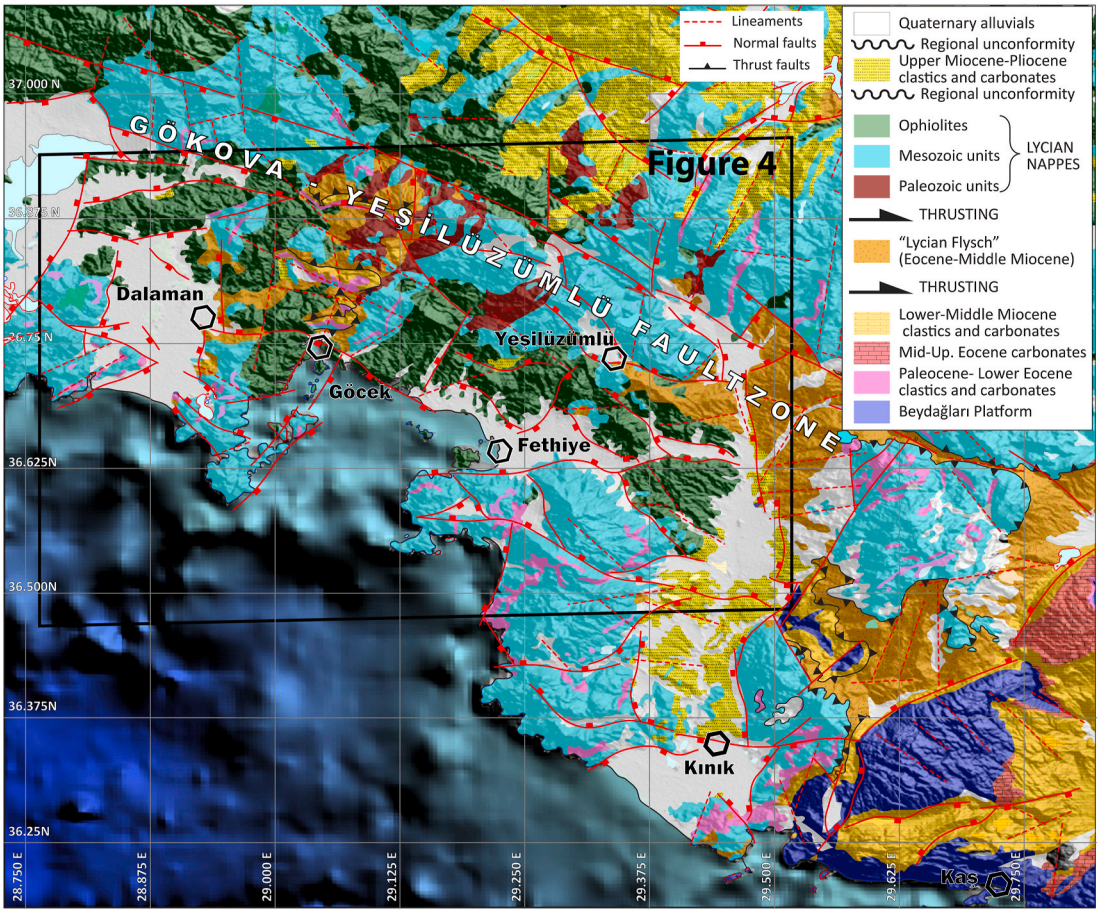

Fig. 2. Simplified geological and structural map of the Study Area (adopted from 1:500.000 geological map of MTA, 2002).

NE-SW trending allochthonous units tectonically overlie the Eocene Nummulitic carbonates and Eocene-Early Miocene turbidites, Lycian Flysch (Blumenthal 1963; Poisson, 1984) of the Menderes Massif that constrains the timing of their emplacement (Okay, 2001). The age of the turbidites and thrusts become younger from west to east, as young as end Serrvallian (beginning of late Miocene) (Hayward, 1984) and they are sandwiched between Lycian Nappes in the west and the Beydağları platform in the east that constitutes structurally the lowest unit below the Lycian Thrust Front (Fig. 1b).

The stratigraphical units important for the context of this paper involve Quaternary alluvial unit. They are developed along major streams in the region and some small graben and half-graben like structures in the downthrown blocks of the normal faults, as well as in the off-sehor e areas. Late Miocene and Pliocene units are largely missing in the study area, and therefore, Quaternary alluvial units are the main stratigraphic markers for dating the events in the study area.

3. Active tectonics and seismicity

The study area is situated close to the northern tip of the Pliny-Strabo Trench, one of the seismically active regions in SW Turkey. It extends along NE-SW direction between the Fethiye-Göcek Bay and Sultan Mountains for a length of about 310 km and with a width of 40–50 km (Poisson et al., 2003; Elitez, 2010). It is argued that the fault zone lacks a continuous master fault on the surface; instead, it comprises various linear, near-vertical fault segments comprising oblique-slip normal faults trending in a NE-SW direction, even though the detailed kinematics of the fault zone has not been resolved yet (e.g., Dumont et al., 1979; Eyidoğan and Barka, 1996; Barka and Reilinger 1997; Taymaz et al., 1991; Taymaz and Price, 1992; Koçyiğit et al., 2000; Alçiçek et al., 2006; Hall et al., 2014; Tiryakioğlu et al., 2013; Alçiçek et al., 2013; Kaymakçı et al., 2014; Kiratzi et al., 2013; Özbakır et al., 2017Alçiçek, 2007; Alçiçek and ten Veen, 2008; ten Veen et al., 2009). Another notable active structural element of the region is a WNW-ESE-trending fault zone, which is formed as a combination of numerous en-échelon

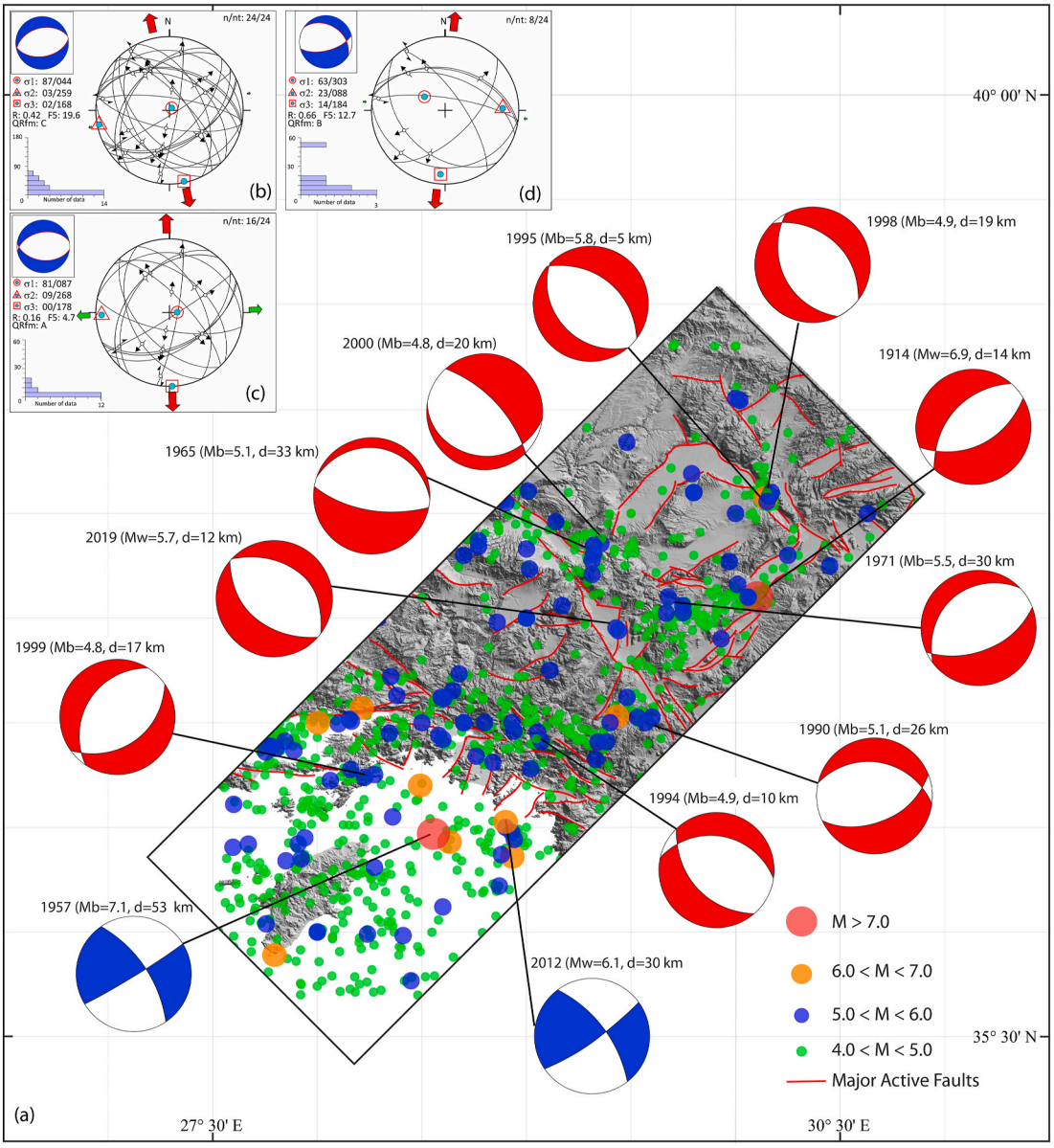

Fig. 3. a) Spatial distribution of earthquakes M > 4 and the focal mechanism solutions of some of them. b-d) the orientation of principal stress orientations based on the moment tensor results. b) whole data, c) set-1solution for the data with less than 30° miss-fit angle, d) set-2 stress configuration for the remaining data. Note NE-SW directed extension for all the solutions.

normal faults transecting the NE-SW-trending faults and is referred as Gökova-Yeşilüzümlü Fault Zone by Hall et al. (2014) (Fig. 2).

Our study area is known as the Göcek Window (Hayward, 1984) where the Eocene sequences of Lycian Flysch is exposed below the Lycian Nappes, which comprises stacked thrust sheets of platform carbonates and ophiolitic units (Fig. 2).

According to the Disaster and Emergency Management Authority (AFAD) earthquake catalogues, there are hundreds of earthquakes (M>=4) occurred around the Fethiye-Göcek Bay during the instrumental period between 1900 and 2017 years. During the past century, five large earthquakes (M>=5) were recorded, and they have resulted in severe ground motions at the study area. These are (1) Ms 5.2 earthquake in 1905, (2) Ms 5.4 earthquake in 1943, (3) Ms 5.3 earthquake in 1959, (4) Ms 5.3 earthquake in 1963, and (5) Ms 5.0 earthquake in 1967. In addition, according to the European Archive of Historical Earthquake Data (AHEAD), there are also historical earthquakes reported around the study area. The most prominent ones include 1851 (M = 6.8) and 1870 (M = 6.0) earthquakes. Fig. 3 shows the distribution of both instrumentally recorded and historical earthquakes in the region (Table 1) and configuration of principal stresses constructed using the major earthquake moment tensor solutions as input (Fig. 3b). Based on available focal mechanism solutions, the earthquakes occurred on normal faults in the Fethiye-Göcek Bay and its vicinity, whereas the off-shore earthquakes are associated with strike-slip faults.

4. Kinematic analysis

Kinematic studies include mapping the faults and conducting paleostress analysis on each fault using fault-slip data. Paleostress analysis involves a collection of fault data sets in the field and reconstruction of paleostress configurations for each sampling site (Angelier, 1994; Simón, 2019). The data sets include the attitude of the fault plane and the slickenside orientations, as well as the sense of motion.

The study area was investigated by using available geological data, satellite, and airborne imagery. In order to determine areas for detailed study and kinematic data collection, lineament maps were prepared. Lineaments are defined as mappable rectilinear or slightly curvilinear surface features, which are recognizably different from the patterns of adjacent ones and presumably reflect subsurface phenomena (O'Leary et al., 1976). Although various automatic lineament extraction techniques using digital elevation models (DEM) and other satellite or airborne imagery are available (e.g., Ganas et al., 2005), we preferred to employ visual interpretation techniques by on-screen digitizing to better judge the origin of the detected lineaments using their context with respect to geological units and the landforms. These techniques were applied to DEMs generated from 1/25.000 scale topographical maps, enhanced Landsat TM imagery, and 60 cm resolution satellite imagery of GoogleEarth.

During the ground-truthing phase, each lineament was visited in the field, and the ones with fault planes and slickensided surfaces are-classified as faults, and are categorized based on the senses of motions obtained from kinematic indicators developed along with them. On the other hand, linear to curvilinear prominent topographic scarps without any kinematic indicators were kept as lineaments in the final map.

As seen in Fig. 4, the traces of faults have bimodal distribution trending predominantly in E-W to N70W and N30E directions while the lineaments are generally scattered, but they are loosely clustered in E-W to NW-SE and N20E directions. It is important to note that both main trends of the normal faults and the lineaments are subparallel to the Gökova-Yeşilüzümlü Fault Zone.

4.1. Paleostress analysis

Fault slip data measurements were conducted both on the mainland and also each of the islands in the Fethiye and Göcek bays. The attitudes of each fault plane and slickensides were recorded using eGEO Compass Pro Application, developed by Marc Foi (2010, updated on 31 May 2016). The "pro" version of the application available in Google Play was installed on Samsung Note 4 and Samsung Galaxy S7 smartphones. The app can record both the fault plane and pitch/rake of slickensides on a single click in a few seconds. During the measurement of slickensides, GPS accuracy and instant magnetic declination variation were also recorded by the software.

Recent studies (e.g., Allmendinger et al., 2017; Novakova and Pavlis, 2017; Lee et al., 2013) about the reliability of smartphones in data collection have demonstrated that they can be used safely in the collection of orientation data and data capture in the field. However, a thorough and very frequent calibration of the compass of the phone is advised. In this regard, it is important to note that during the data collection, both smartphones were calibrated for each site or after 100 measurements, just to be on the safe side. As a sampling strategy, the size of the sampling stations (sites) was kept as small as possible for the purpose of obtaining structurally homogeneous domains, and each fault was sampled at least at three different locations along its trace separated by few kilometres apart in order not to avoid any kinematic change along the trace of the same fault. For each sampling site, the attitude of the fault plane, the pitch/rake of the slickenside, the relative sense of each moment in the case of overprinting slickensides were noted with

Table 1
Parameters of earthquakes focal mechanism solutions and resultant stress configurations.

Date D/M/Y	Lat. (N)	Lon. (E)	Depth (km)	Magnitute (type)	Plane 1			Plane 2			Reference
					Strike	Dip	Rake	Strike	Dip	Rake	
03.10.1914	37.9	30.4	14	6.9 (Mw)	222	42	−10	64	50	−75	Shebalin et al., 1974
25.04.1957	36.47	28.56	53	7.1 (Mb)	58	85	19	325	71	174	Tan et al., 2008
13.06.1965	37.85	29.32	16	5.1 (Mb)	101	70	−90	281	20	−90	Tan et al., 2008
12.05.1971	37.64	29.72	23	5.5 (Mb)	222	42	−107	64	50	−75	Tan et al., 2008
18.07.1990	37	29.57	8	5.1 (Mb)	66	52	−114	282	44	−62	Tan et al., 2008
13.11.1994	36.92	29.05	12	4.9 (Mb)	138	55	−66	280	42	−120	Tan et al., 2008
01.10.1995	38.06	30.15	8	5.8 (Mb)	135	40	−105	334	52	−78	Tan et al., 2008
04.04.1998	38.1	30.15	6	4.9 (Mb)	154	45	−74	311	47	−106	Tan et al., 2008
05.10.1999	36.75	28.24	15	4.8 (Mb)	55	48	−75	213	44	−106	Tan et al., 2008
21.04.2000	37.88	29.36	6	4.8 (Mb)	316	72	−75	96	23	−128	Tan et al., 2008
10.06.2012	36.53	28.9	30	6.1 (Mw)	10	81	14	278	76	171	AFAD, 2019
20.03.2019	37.44	29.43	12	5.7 (Mw)	28	48	−91	310	42	−89	AFAD, 2019
CONFIGURATION OF CONSTRUCTED REGIONAL STRESSES											
Data	n	nt	σ_1		σ_2		σ_3		R	Regime	
			Plunge	Azimuth	Plunge	Azimuth	Plunge	Azimuth			
All data	24	24	87	044	03	259	02	168	0.42	N–S Extension	
Set 1	16	24	81	087	09	268	00	178	0.16	N–S Extension	
Set 2	8	24	63	303	23	088	14	184	0.66	N–S Extension	

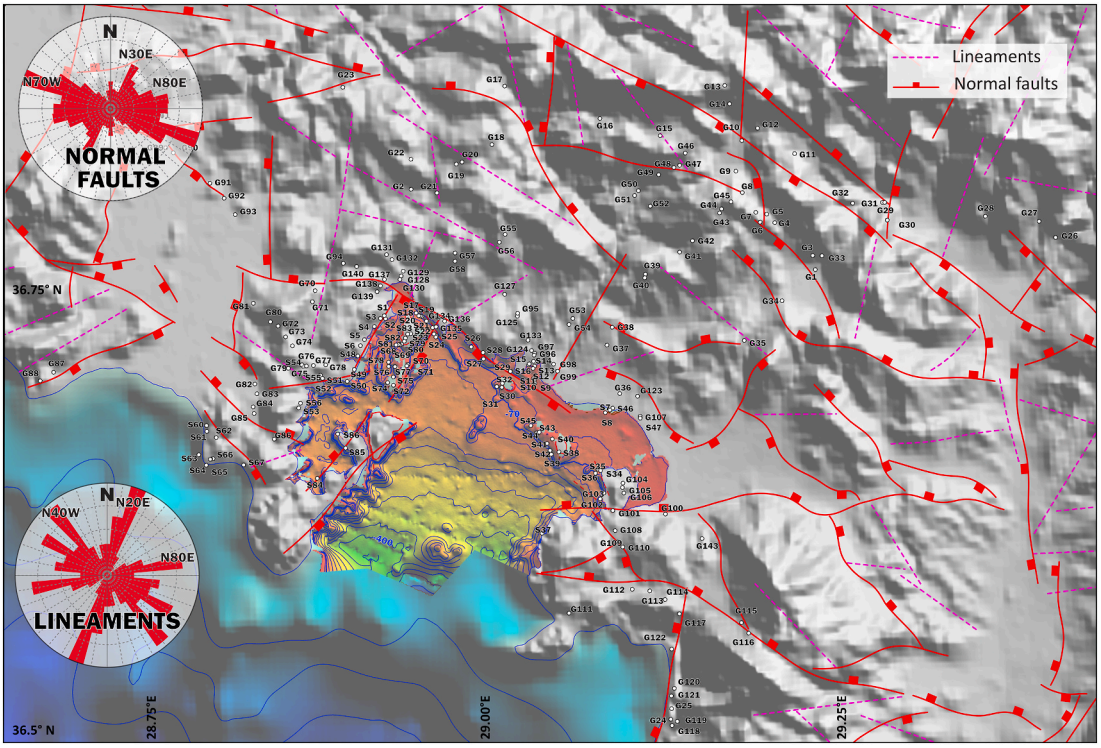

Fig. 4. Structural map of the study area and length weighted rose diagrams for the normal faults, and the lineaments. Note the clustering of normal faults in E-W to N70W and N30E directions and dispersion in the orientations of the lineaments.

their geographic locations and photographs of each fault, and the site was documented (Figs. 5–8). The direction of relative displacement on each fault plane was determined by kinematic indicators on the fault plane. On most of the faults, grooves, chatter marks, tools marks, and fibrous minerals and gash veins were extensively developed.

4.2. Results of paleostress analysis

In total, 14921 slip data from 216 different locations were collected, and they were analyzed using Win_Tensor V5.8.8 software developed by Delvaux and Sperner (2003). After the analysis, 14710 of the measured fault-slip data produced reliable results. The remaining 211 data (~0.012%) were found to be spurious, and they were excluded. The spurious data have been recognized only in a few sites, and they are resulted from either impossible angles or slip senses with respect to the majority of the rest of the data in each site. For the analysis of each data sets, the R-Optimized routine was used (Delvaux and Spener, 2003). The obtained stress configurations are given in Table 2 and Fig. 9 (see also Supplement A). In Fig. 10, horizontal components of minor stress axis (σ_3) were depicted in order to illustrate their relationship with the associated faults. Collective analysis of all of the constructed paleostress configurations indicates near-vertical orientations of major stress (σ_1) while intermediate (σ_2) and minor stress (σ_3) are not constrained in any direction, and they are almost scattered in all directions. Such stress configurations indicate uniaxial stress conditions under which a multi-directional extension takes place. However, elongation of σ_3 mean direction about the N75W direction indicates that the dominant extension direction is about NNW-SSE.

Due to the lack of Neogene units in the region, the temporal order of the fault motions could not be established precisely. However, most of the sampled faults control the deposition of the Quaternary units in the region, which implies that these faults have been active until recently, and therefore, such faults were classified as active faults whereas the ones which do not have any direct contact with the Quaternary units were classified as other faults. Nevertheless, almost all of the constructed paleostress configurations collectively indicate extensional deformation, although NW-SE striking normal faults dominate the on-land areas.

4.3. Analysis of moment tensor solutions

Moment tensor solutions obtained from the literature (Table 1) are analyzed with WinTensor software, in order to obtain regional stress pattern. For this purpose, all the movement and auxiliary planes, and magnitudes of the earthquakes are used as input data (24 planes in total). First, the whole data is analyzed using rotational optimization routine of the software. The results indicate vertical major principal stress ($\boldsymbol{\sigma_1}$ = 044N/87), while other stresses are horizontal and are oriented $\boldsymbol{\sigma_2}$: 259N/03 $\boldsymbol{\sigma_3}$: 168N/02 directions (Fig. 3b). In this solution, the miss-fit angles reach up to 75° for some of the planes. Then the data is re-analyzed by taking the maximum allowed miss-fit angle 30°. The first set indicates vertical major principal stress ($\boldsymbol{\sigma_1}$: 087N/81) and horizontal intermediate ($\boldsymbol{\sigma_2}$:268N/09) and minor ($\boldsymbol{\sigma_3}$:178N/00) principal stresses (Fig. 3c). The second set produced subvertical ($\boldsymbol{\sigma_1}$:303N/63) and sub-horizontal intermediate ($\boldsymbol{\sigma_2}$:088N/23)and minor ($\boldsymbol{\sigma_3}$:184N/14) principal stress orientations (Fig. 3d). The results for the whole data and the first set are almost similar. However, set 2 has the largest discrepancy. Nevertheless, all of the solutions indicate almost N–S directed extension for the study area.

5. Seismic interpretation

In order to determine the current activity, characteristics, and orientation of the faults developed in Fethiye-Göcek Bay, 2D seismic reflection data transecting the probable geological structures developed in the bay were interpreted. During the interpretation, the most prominent and continuous reflectors were picked in the time domain. The faults were interpreted on each seismic line by using picked horizons and seismic layer terminations. Then the interpreted horizons and faults were correlated from one section to another throughout the bay. As a

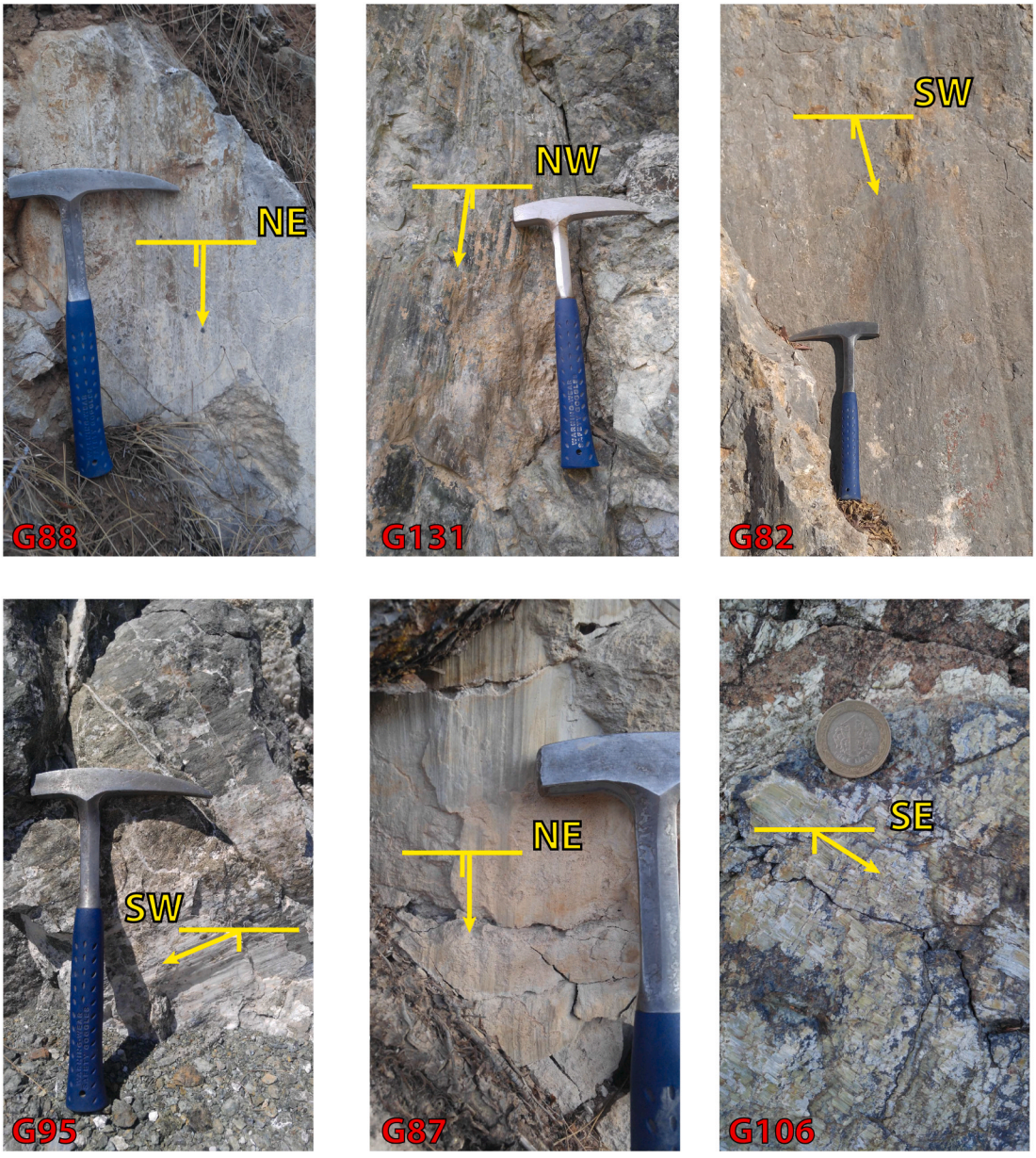

Fig. 5. Slickensides on various fault planes. Arrows indicate the sense of slip of the hanging-wall block. Note that G95 is a NE-SW striking fault with dextral component and G106 is a NW-SE striking fault with a sinistral component. All others are normal faults.

result, the sea-bottom projections of the faults were mapped out, and they were used to improve the understanding of spatial distributions and activity of the faults developed in the Fethiye-Göcek Bay.

5.1. Seismic data acquisition and processing

In total, 228 km long single-channel seismic reflection profiles along 32 lines were used in this study (Fig. 11a) In order to increase the signal to noise ratio, SeisSpace/Promax software developed by Landmark/Halliburton was used. The horizontal offset between traces was kept at 2 m (horizontal resolution), which means that seabed and units below were sampled every 2 m along tracks while the vertical resolution is ~40 cm since the applied dominant frequency was 1000 Hz.

The positions of the shot points were determined by GPS measurements taken simultaneously during the survey. For the bathymetric map of the bay integration and linear interpolation of seismic and independent depth measurements during the survey were used. For two-way-time to depth conversion, the velocity of the water was taken as 1500 m/s. The shelf break is located ~7 km away from the coastline, where the depth of bathymetry rapidly increases from 170 m to 270 m. In addition, local highs on the seismic sections correspond to high-velocity basement units and are emphasized on the bathymetric image.

5.2. 2D-seismic interpretation

The seismic interpretations, including the horizon picking and fault tracing as well as extraction of surface map projection of faults, were performed by IHS-Kingdom Suite software provided through Academic License Act. The interpretation processes were carried out in two main stages: defining and picking the key horizons and fault interpretation.

5.2.1. Defining and picking the key horizons

Due to the lack of well data, no time to depth conversion was applied on the seismic data, and therefore the interpretations were performed on time-domain data, and six horizons were picked in total. Mainly region-wide traceable high amplitude reflections, seismic stratigraphic

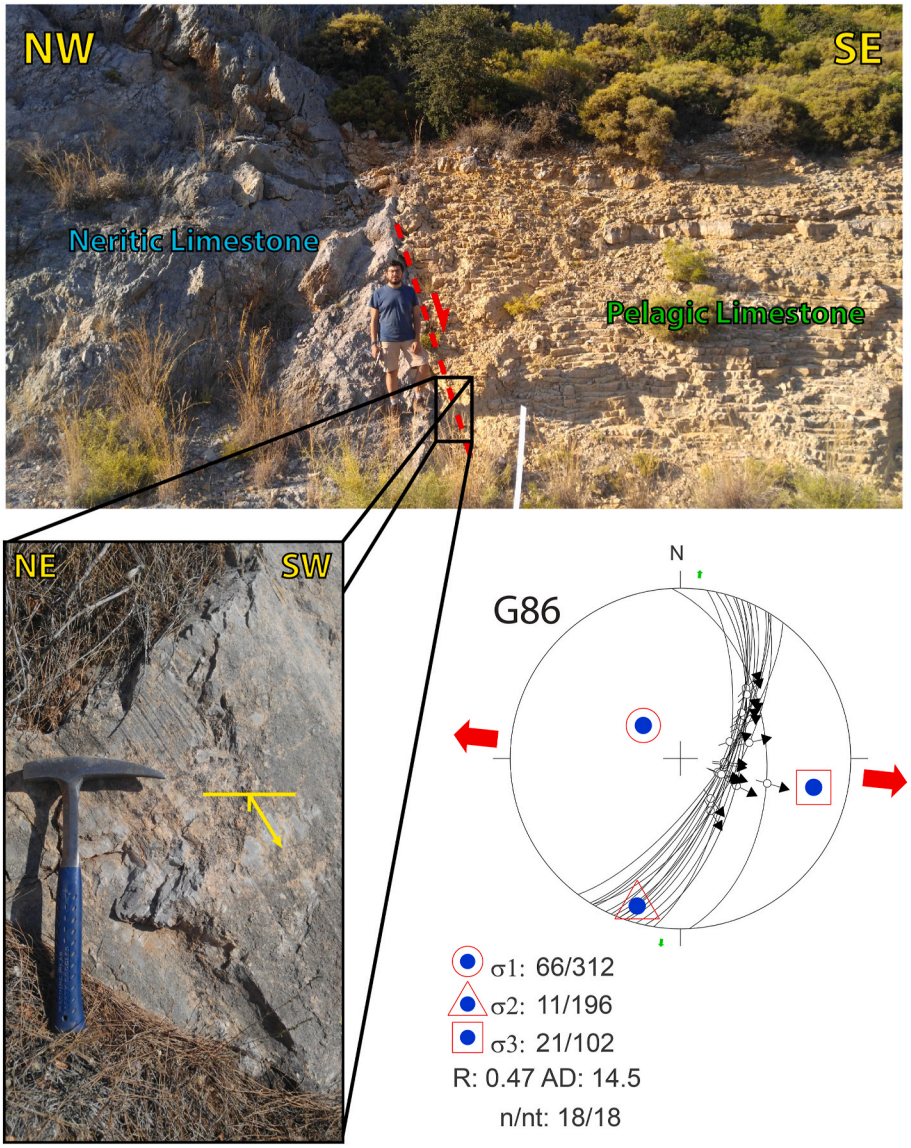

Fig. 6. The fault, juxtaposing neritic and pelagic limestone at the site G86 along the hanging wall and footwall blocks respectively and its constructed paleostress orientations.

characteristics, and seismic facies such as on-lap, down-lap, shingle patterns, etc. are used for horizon picking. As expected, the thickness of the sections above the acoustic basement is highest on the southern side of the shelf break, towards the deeper part of the bay (Fig. 11a).

5.2.2. Fault interpretation

The faults were identified and mapped by reflection offsets in seismic sections and the morphological expressions of the surfaces. Each fault on the individual seismic section was mapped (e.g., Fig. 12). Then, each fault was correlated to the adjacent sections by a jump-correlation in order to map them on the sea bottom. In this process, the bathymetric map, the geometry of adjacent horizons, and fault geometries were taken into consideration. The on-land continuations of faults were deduced from bathymetry. Faults that do not cut the sea bottom were mapped separately. A total of 108 fault interpretations were performed on seismic sections. During correlations of major faults, smaller antithetic or synthetic faults, which are not persistent across the seismic sections, were neglected. The remaining 84 faults were correlated and mapped on the seabed (Fig. 11a).

5.3. Seismic interpretation results

The orientation of the interpreted faults on the seismic sections scatter around 90° between N50W to N40E while the dominant direction is N40E. However, the dominant direction of the on-land faults is N50W, almost parallel to the faults at the northern margin of the bay, while the faults in the deeper parts of the bay are oriented NE-SW. It seems that NW-SE striking faults are associated with the Gökova-Yeşilüzümlü Fault Zone while NE-SW striking faults are the northernmost continuation of Pliny-Strabo system (Ocakoğlu, 2012).

The paleostress reconstruction analysis performed on on-land faults revealed that almost all faults are normal in character and associated with dominant NW-SE oriented extensional deformation. Likewise, the type of the faults which were interpreted from seismic sections has very strong vertical normal components, i.e., dip-slip component, which we infer that they are also normal faults (Fig. 12).

In addition to faults cutting the seabed, some of the faults cut only the basement and the lower part of the seabed deposits (Fig. 13). In order to determine their latest activity, ^{137}Cs measurements obtained from a gravity core (Avşar et al., 2017) are used (Fig. 11c). The peak in 1963 corresponding to atmospheric nuclear weapon tests is located

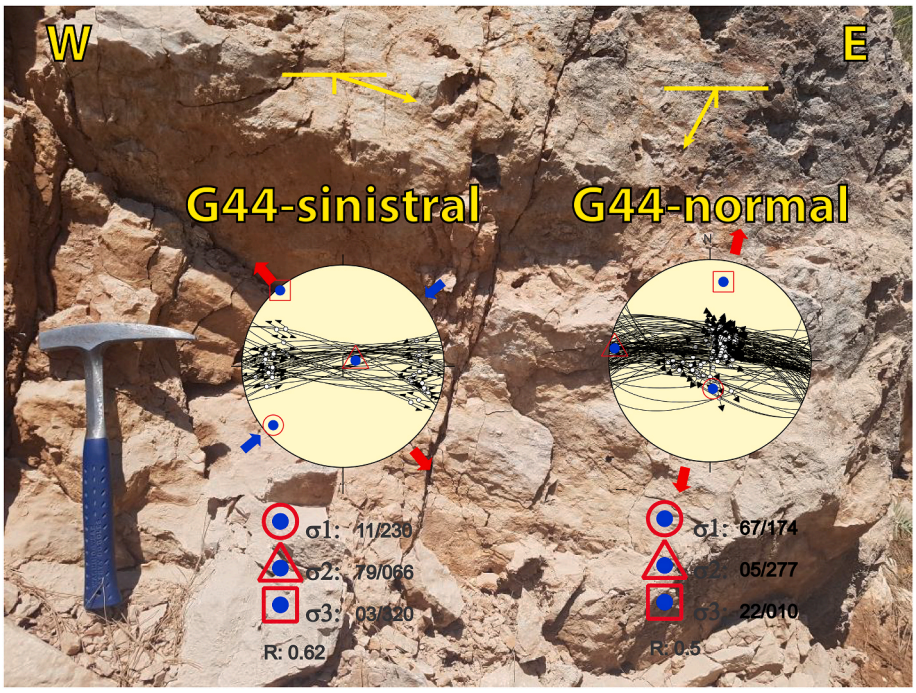

Fig. 7. Overprinting slickensides and their paleostress configurations.

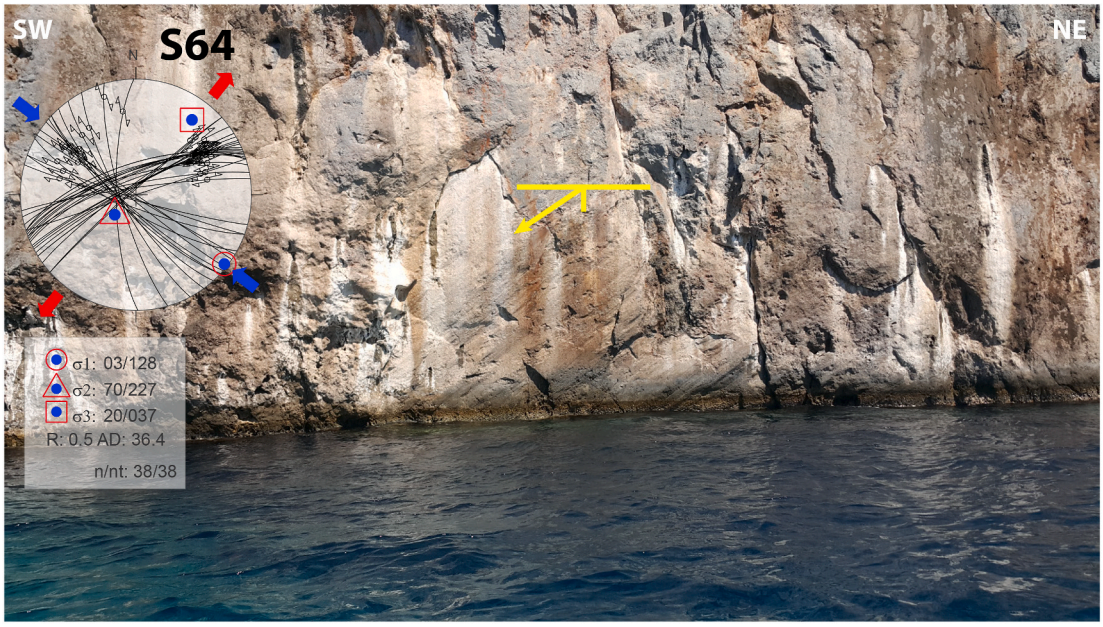

Fig. 8. NE-SW-trending dextral strike-slip fault on cliffs and their paleostress configuration.

around 21 cm depth, which yields 4 mm/yr sedimentation rate for the top-most part of the recent deposits at the coring location. On the seismic line FT14-09, the closest line to the coring site, the thickness of the sedimentary sequence calculated to be ~14m (Fig. 11b). For the calculations, the seismic velocity of water and the average interval velocity of unconsolidated wet sediments were taken as 1500 m/s and 2000 m/sec, respectively (Sharma, 1997). Hence, the required time for the deposition of 14 m of sediments is found to be around 3500 years, which might be slightly more than that if compaction of sediments is taken into account. This indicates that even the faults that do not cut the upper parts of the recent sediments at the bottom of the sea, since they cut their lower parts, therefore some of the mapped faults in the seismic sections had activity within the last 3500 years. This implies that most of these faults can be classified as active faults since they have been active during the Holocene Epoch.

6. Discussion

The integration of seismic interpretation and kinematic studies revealed that the Fethiye-Göcek Bay area is under the influence of extensional tectonics. Most of the structures, both on-land and off-shore, are normal faults with local minor strike-slip components. The occasionally developed faults with strong strike-slip components (slickenside pitches smaller than 45°) are not constrained to any particular direction

Table 2
Detailed information about constructed paleostress orientations per site [See Delvaux and Sperner (2003) for the full account of the paleostress inversion methodology.]. (see Supplement A for further detailed information).

NO	ID	Long	lat	n	σ_1		σ_2		σ_3		R	Reg	Stress Regime	Misfit Value	QRw	QRt
					P	D	P	D	P	D						
1	G1	29.2349	36.7567	28	67	130	19	341	11	247	0.24	NF	Radial Ext.	4.5	A	E
2	G2	28.9491	36.8075	45	80	346	10	166	0	256	0.35	NF	Pure Ext.	12.5	C	C
3	G3	29.2333	36.7648	33	71	299	18	127	2	36	0.18	NF	Radial Ext.	5.9	A	E
4	G4	29.2068	36.7841	59	68	27	2	292	22	201	0.25	NF	Pure Ext.	7.1	A	E
5	G5	29.2013	36.7890	168	76	133	14	312	0	42	0.06	NF	Radial Ext.	8.5	A	E
6	G6	29.1965	36.7845	73	84	269	5	132	4	42	0.16	NF	Radial Ext.	14.3	C	C
7	G7	29.1936	36.7902	98	55	118	34	308	5	215	0.18	NF	Radial Ext.	6.3	A	E
8	G8	29.1844	36.8016	47	67	89	20	239	10	333	0.66	NF	Pure Ext.	11.1	B	D
9	G9	29.1801	36.8140	122	87	168	2	35	2	305	0.01	NF	Radial Ext.	11.7	B	E
10	G10	29.1848	36.8313	79	35	77	46	302	24	185	0.15	NS	Oblq. TrT.	8.9	A	E
11	G11	29.2221	36.8232	87	71	336	18	134	7	226	0.03	NF	Radial Ext.	8.5	A	D
12	G12A	29.1963	36.8389	141	74	195	15	356	5	87	0.93	NF	St-S. Ext.	11.1	B	C
13	G13	29.1736	36.8629	31	52	86	27	216	25	320	0.1	NS	Oblq. Ext.	9	A	C
14	G14	29.1767	36.8524	17	68	105	5	209	21	301	0.32	NF	Pure Ext.	7.4	B	C
15	G15	29.1269	36.8351	39	74	298	15	108	2	199	0.56	NF	Pure Ext.	14.8	C	C
16	G16	29.0843	36.8457	6	80	163	9	331	2	61	0.5	NF	Pure Ext.	4.3	D	D
17	G17	29.0172	36.8653	62	33	37	51	254	19	139	0.02	NS	Oblq. TrT.	7.9	A	E
18	G18	29.0072	36.8321	123	74	200	5	91	15	359	0.49	NF	Pure Ext.	8.8	A	D
19	G19	28.9857	36.8226	48	88	142	2	331	0	241	0.14	NF	Radial Ext.	7.8	A	E
20	G20	28.9816	36.8214	128	78	3	7	236	9	144	0.39	NF	Pure Ext.	10.7	B	E
21	G21	28.9674	36.8052	27	80	189	2	87	10	356	0.29	NF	Pure Ext.	9.2	B	C
22	G22	28.9495	36.8247	28	88	342	2	163	0	73	0.07	NF	Radial Ext.	9	A	C
23	G23	28.9021	36.8665	92	79	196	2	95	11	5	0.33	NF	Pure Ext.	9.6	B	E
24	G24	29.1253	36.5023	74	88	232	2	54	0	324	0.11	NF	Radial Ext.	9.5	B	C
25	G25	29.1260	36.5083	29	54	224	34	24	9	121	0.24	NS	Oblq. Ext.	18.4	E	E
26	G26	29.4060	36.7718	144	83	140	2	33	7	302	0.36	NF	Pure Ext.	15.1	D	D
27	G27A	29.3946	36.7812	56	78	334	11	129	5	220	0.53	NF	Pure Ext.	17.3	D	D
28	G28	29.3565	36.7848	81	86	3	1	112	3	202	0.25	NF	Pure Ext.	12.4	C	C
29	G29	29.2853	36.7941	80	84	120	6	298	0	29	0.13	NF	Radial Ext.	6	A	E
30	G30	29.2868	36.7840	72	80	113	7	335	7	245	0.01	NF	Radial Ext.	6.8	A	E
31	G31	29.2837	36.7941	96	83	245	6	50	2	140	0.36	NF	Pure Ext.	8	A	B
32	G32	29.2626	36.7941	27	84	286	3	44	6	134	0.51	NF	Pure Ext.	9	B	E
33	G33	29.2398	36.7646	127	74	332	6	83	15	174	0.01	NF	Radial Ext.	10.5	B	E
34	G34	29.2107	36.7394	108	87	131	0	33	3	303	0.54	NF	Pure Ext.	13.1	C	C
35	G35	29.1833	36.7173	80	70	38	16	254	11	161	0.11	NF	Radial Ext.	14.3	C	E
36	G36	29.0941	36.6886	71	83	202	7	39	2	309	0.27	NF	Pure Ext.	6.4	A	E
37	G37	29.0859	36.7164	149	89	299	0	203	1	113	0.18	NF	Radial Ext.	11	B	D
38	G38	29.0899	36.7265	38	83	27	7	222	2	132	0.67	NF	Pure Ext.	13.6	C	C
39	G39	29.1137	36.7543	70	72	234	14	14	11	107	0.19	NF	Radial Ext.	8.3	A	E
40	G40	29.1142	36.7563	48	63	107	6	208	27	301	0.32	NF	Pure Ext.	4.7	A	E
41	G41	29.1389	36.7685	103	42	30	42	246	19	138	0.49	NS	Oblq. TrT.	14.3	C	C
42	G42	29.1482	36.7748	39	80	279	8	61	6	151	0.01	NF	Radial Ext.	9.7	B	E
43	G43	29.1678	36.7903	98	80	169	6	296	8	27	0.09	NF	Radial Ext.	5	A	E
44	G44A	29.1693	36.7926	123	88	146	1	257	2	347	0.01	NF	Radial Ext.	8.3	A	E
45	G45	29.1762	36.7965	34	64	82	25	244	7	337	0.31	NF	Pure Ext.	6.1	A	E
46	G46	29.1444	36.8249	121	81	63	8	219	4	310	0.19	NF	Radial Ext.	7.2	A	E
47	G47	29.1403	36.8180	86	69	86	9	201	18	294	0.21	NF	Radial Ext.	12	B	E
48	G48	29.1361	36.8168	97	81	143	2	244	9	334	0.12	NF	Radial Ext.	8.2	A	E
49	G49	29.1252	36.8129	76	65	48	24	214	5	307	0.34	NF	Pure Ext.	15.2	D	D
50	G50	29.1105	36.8040	85	35	155	54	319	8	60	0.66	NS	Oblq. TrT.	7.1	A	E
51	G51	29.1075	36.8010	147	60	144	26	294	13	31	0.02	NF	Radial Ext.	17.6	D	D
52	G52	29.1187	36.7951	68	70	214	12	90	16	356	0.59	NF	Pure Ext.	10.5	B	C
53	G53	29.0621	36.7320	84	79	129	11	315	1	224	0.91	NF	St-S. Ext.	7.6	A	C
54	G54	29.0592	36.7286	102	80	330	6	202	8	111	0.62	NF	Pure Ext.	8	A	E
55	G55	29.0153	36.7807	74	84	19	6	228	3	138	0.32	NF	Pure Ext.	11.2	B	E
56	G56	29.0110	36.7764	35	82	270	7	71	2	161	0.01	NF	Radial Ext.	7.3	A	E
57	G57	28.9794	36.7708	90	83	98	4	335	6	245	0.1	NF	Radial Ext.	10.1	B	D
58	G58	28.9793	36.7661	29	83	356	7	202	3	111	0.01	NF	Radial Ext.	9.6	B	D
59	G70	28.8795	36.7509	32	76	5	14	172	3	263	0.45	NF	Pure Ext.	8.7	A	D
60	G71	28.8774	36.7446	22	65	166	24	328	7	61	0.41	NF	Pure Ext.	6.2	B	E
61	G72	28.8527	36.7311	30	61	134	3	38	29	306	0.09	NF	Radial Ext.	6.8	A	E
62	G73	28.8579	36.7248	37	56	163	34	344	1	254	0.31	NF	Pure Ext.	10.2	B	E
63	G74	28.8626	36.7197	17	75	97	6	343	14	252	0.31	NF	Pure Ext.	8.3	B	B
64	G75	28.8689	36.7089	41	83	229	6	15	4	105	0.07	NF	Radial Ext.	8.9	A	D
65	G76	28.8703	36.7082	32	35	114	55	299	3	206	0.86	SS	Ext.St-S.	5.3	A	E
66	G77	28.8772	36.7082	21	36	263	54	82	0	172	0.88	NS	Oblq. TrT.	11.8	B	C
67	G78	28.8860	36.7084	27	54	349	36	165	2	256	0.89	NS	Oblq. Ext.	9.6	B	E
68	G79	28.8595	36.7069	78	88	310	1	75	2	165	0.01	NF	Radial Ext.	13.4	C	D
69	G80	28.8473	36.7336	43	75	9	15	192	1	101	0.04	NF	Radial Ext.	11.7	B	E
70	G81	28.8354	36.7444	17	59	30	3	125	31	216	0.08	NF	Radial Ext.	8.9	B	E
71	G82	28.8354	36.6983	95	87	328	2	179	1	89	0.26	NF	Pure Ext.	6	A	E
72	G83	28.8368	36.6927	13	59	102	9	356	29	261	0.44	NF	Pure Ext.	7.5	C	E

(*continued on next page*)

Table 2 (*continued*)

NO	ID	Long	lat	n	σ_1		σ_2		σ_3		R	Reg	Stress Regime	Misfit Value	QRw	QRt
					P	D	P	D	P	D						
73	G84	28.8339	36.6853	39	59	94	1	185	31	275	0.17	NF	Radial Ext.	6.6	A	E
74	G85	28.8345	36.6815	55	68	128	13	5	18	271	0.45	NF	Pure Ext.	14	C	D
75	G86	28.8485	36.6667	18	81	339	8	180	3	90	0.11	NF	Radial Ext.	15.2	D	E
76	G87	28.6928	36.7071	29	89	91	0	196	1	286	0.06	NF	Radial Ext.	11.6	B	C
77	G88	28.6832	36.7024	81	70	23	10	263	17	170	0.26	NF	Pure Ext.	7.7	A	E
78	G89	28.7753	36.8340	44	66	53	22	259	9	165	0.22	NF	Radial Ext.	7.3	A	C
79	G90	28.7806	36.8311	69	66	296	16	166	17	70	0.04	NF	Radial Ext.	7.5	A	E
80	G91	28.8062	36.8133	104	68	313	16	87	15	181	0.28	NF	Pure Ext.	9.8	B	D
81	G92	28.8161	36.8046	82	85	75	4	218	3	309	0.05	NF	Radial Ext.	7.7	A	E
82	G93	28.8238	36.7951	76	75	29	15	213	1	122	0.6	NF	Pure Ext.	13.5	C	D
83	G94	28.8999	36.7662	45	83	112	7	272	3	2	0.3	NF	Pure Ext.	6.7	A	E
84	G95	29.0230	36.7356	67	28	231	56	14	17	131	0.63	SS	Pure St-S.	12.9	C	D
85	G96	29.0340	36.7116	65	70	233	20	62	3	331	0.83	NF	St-S. Ext.	6.1	A	C
86	G97	29.0344	36.7127	92	66	330	22	126	9	220	0.3	NF	Pure Ext.	10.3	B	E
87	G98	29.0477	36.7062	66	54	352	35	161	5	255	0.36	NS	Oblq. Ext.	11.1	B	E
88	G99	29.0504	36.7022	56	56	329	28	109	19	209	0.31	NF	Pure Ext.	9.5	B	E
89	G100	29.1247	36.6193	26	67	29	12	149	19	243	0.06	NF	Radial Ext.	12	B	D
90	G101	29.0874	36.6220	27	77	98	4	205	12	296	0.01	NF	Radial Ext.	11.8	B	D
91	G102	29.0787	36.6287	53	82	142	7	286	5	16	0.04	NF	Radial Ext.	11.2	B	D
92	G103	29.0814	36.6321	58	83	128	6	278	4	8	0.38	NF	Pure Ext.	6.5	A	E
93	G104	29.0951	36.6375	46	69	185	21	17	4	285	0.44	NF	Pure Ext.	12.6	C	D
94	G105	29.0946	36.6350	47	51	238	31	18	21	121	0.49	NS	Oblq. Ext.	5.8	A	E
95	G106	29.0955	36.6319	44	52	190	27	58	24	315	0.34	NS	Oblq. Ext.	7.8	A	E
96	G107	29.1083	36.6743	44	88	63	2	228	1	318	0.41	NF	Pure Ext.	9.8	B	D
97	G108	29.0888	36.6105	62	65	81	3	344	25	253	0.23	NF	Radial Ext.	3.1	A	E
98	G109	29.0906	36.6040	82	74	91	5	200	15	292	0.06	NF	Radial Ext.	5.5	A	E
99	G110	29.0939	36.6011	39	70	340	8	95	17	187	0.2	NF	Radial Ext.	6.7	A	E
100	G111	29.0549	36.5640	70	81	88	7	308	6	217	0.04	NF	Radial Ext.	11.9	B	D
101	G112	29.1000	36.5768	44	81	192	8	37	3	306	0.23	NF	Radial Ext.	3.4	A	E
102	G113	29.1124	36.5757	27	65	197	25	21	2	291	0.55	NF	Pure Ext.	6.5	A	E
103	G114	29.1231	36.5706	66	86	160	0	66	4	336	0.01	NF	Radial Ext.	4.1	A	E
104	G115	29.1768	36.5564	25	71	47	19	226	0	316	0.75	NF	Pure Ext.	16.3	D	D
105	G116	29.1817	36.5503	47	71	123	18	282	6	14	0.13	NF	Radial Ext.	9.7	B	E
106	G117	29.1330	36.5622	134	81	215	8	12	3	103	0.15	NF	Radial Ext.	6.3	A	E
107	G118	29.1260	36.4987	17	76	86	13	258	2	349	0.37	NF	Pure Ext.	9.4	B	E
108	G119	29.1299	36.5009	67	54	304	16	189	31	89	0.22	UF	Oblq. Ext.	9.5	B	E
109	G120	29.1260	36.5155	72	87	167	3	16	1	286	0.27	NF	Pure Ext.	7.1	A	E
110	G121	29.1283	36.5198	76	28	108	60	313	11	204	0.13	SS	Comp. St-S.	9	B	E
111	G122	29.1269	36.5423	48	75	38	6	152	14	243	0.3	NF	Pure Ext.	8	A	D
112	G123	29.1067	36.6869	97	71	103	14	240	12	333	0.32	NF	Pure Ext.	10.7	B	E
113	G124	29.0323	36.7142	88	85	239	5	68	1	338	0.05	NF	Radial Ext.	6.2	A	E
114	G125	29.0227	36.7339	82	63	328	21	187	16	91	0.24	NF	Radial Ext.	5.4	A	E
115	G127	29.0140	36.7466	55	83	215	6	14	2	104	0.16	NF	Radial Ext.	9.5	B	E
116	G128	28.9408	36.7583	57	80	299	10	115	1	205	0.25	NF	Pure Ext.	10.3	B	C
117	G129	28.9423	36.7610	52	24	200	37	309	44	85	0.4	TS	Oblq. Comp.	13.9	C	E
118	G130	28.9399	36.7563	86	56	280	1	11	34	101	0.04	NF	Radial Ext.	6.9	A	E
119	G131	28.9307	36.7707	94	74	246	2	148	16	58	0.35	NF	Pure Ext.	10.6	B	E
120	G132	28.9345	36.7677	60	54	154	20	33	29	292	0.44	UF	Oblq. Ext.	3.6	A	E
121	G133	29.0299	36.7201	87	66	153	24	323	3	55	0.01	NF	Radial Ext.	11.2	B	D
122	G134	28.9666	36.7338	133	86	21	3	159	3	250	0.08	NF	Radial Ext.	13.4	C	D
123	G135	28.9648	36.7289	127	87	72	2	195	3	285	0.27	NF	Pure Ext.	9.9	B	D
124	G136	28.9715	36.7311	84	41	6	40	230	24	119	0.14	NS	Oblq. Ext.	9.7	B	D
125	G137	28.9289	36.7565	38	87	334	3	148	0	238	0.01	NF	Radial Ext.	8.2	A	E
126	G138	28.9259	36.7529	107	87	308	0	45	3	135	0.15	NF	Radial Ext.	11.1	B	D
127	G139	28.9235	36.7495	83	80	298	5	175	8	84	0.64	NF	Pure Ext.	9.2	B	D
128	G140	28.9093	36.7641	69	78	258	3	154	11	64	0.39	NF	Pure Ext.	11.2	B	C
129	G141	28.7616	36.8573	52	74	125	15	283	6	14	0.02	NF	Radial Ext.	10.9	B	E
130	G143	29.1502	36.6049	61	57	25	22	154	23	254	0.18	NF	Radial Ext.	5.2	A	E
131	S1	28.9282	36.7358	34	56	19	26	156	20	256	0.01	NF	Radial Ext.	8.2	A	E
132	S2	28.9291	36.7341	95	81	23	6	162	6	252	0.43	NF	Pure Ext.	7.1	A	E
133	S3	28.9255	36.7343	123	89	174	0	268	1	358	0.05	NF	Radial Ext.	11.5	B	D
134	S4	28.9210	36.7298	34	75	118	5	11	15	280	0.39	NF	Pure Ext.	6.3	A	E
135	S5	28.9138	36.7224	66	89	214	0	11	0	101	0.01	NF	Radial Ext.	14.6	C	D
136	S6	28.9109	36.7190	100	55	40	30	256	17	156	0.03	NF	Radial Ext.	7.5	A	D
137	S7	29.0879	36.6795	72	73	274	2	177	17	86	0.12	NF	Radial Ext.	13.1	C	C
138	S8	29.0836	36.6779	28	78	179	7	304	10	35	0.19	NF	Radial Ext.	6.7	A	E
139	S9	29.0342	36.6956	51	73	187	0	277	17	8	0.15	NF	Radial Ext.	7.6	A	E
140	S10	29.0337	36.6972	67	82	59	2	162	8	253	0.29	NF	Pure Ext.	3.9	A	E
141	S11	29.0331	36.6981	56	84	85	4	307	4	217	0.39	NF	Pure Ext.	6.3	A	E
142	S12	29.0331	36.7040	30	73	290	2	194	16	103	0.06	NF	Radial Ext.	5.5	A	E
143	S13	29.0342	36.7053	72	27	42	63	220	1	311	0.39	SS	Pure St-S.	9	B	C
144	S14	29.0335	36.7080	70	83	189	4	321	5	52	0.3	NF	Pure Ext.	6.3	A	E
145	S15	29.0304	36.7067	84	56	149	2	243	34	334	0.08	NF	Radial Ext.	5.3	A	E
146	S16	29.0299	36.7060	104	73	242	17	60	1	150	0.17	NF	Radial Ext.	6.7	A	E

(*continued on next page*)

Table 2 (*continued*)

NO	ID	Long	lat	n	σ_1		σ_2		σ_3		R	Reg	Stress Regime	Misfit Value	QRw	QRt
					P	D	P	D	P	D						
147	s17	28.9509	36.7370	41	81	150	1	53	9	323	0.44	NF	Pure Ext.	10.8	B	C
148	S18	28.9527	36.7354	39	68	133	1	42	22	312	0.16	NF	Radial Ext.	12.8	C	C
149	S19	28.9538	36.7352	40	78	133	10	344	6	253	0.25	NF	Pure Ext.	5.3	B	E
150	S20	28.9549	36.7349	57	81	60	8	263	4	173	0.48	NF	Pure Ext.	8.2	A	C
151	S21	28.9581	36.7323	89	82	119	6	254	6	345	0.39	NF	Pure Ext.	6.4	A	E
152	S22	28.9623	36.7284	75	60	62	25	207	15	304	0.23	NF	Radial Ext.	3.3	A	E
153	S23	28.9632	36.7248	61	75	62	14	265	6	173	0.35	NF	Pure Ext.	9.3	B	E
154	S24	28.9646	36.7230	37	80	271	10	90	0	180	0.49	NF	Pure Ext.	12.4	C	C
155	S25	28.9650	36.7237	49	76	305	12	95	6	187	0.34	NF	Pure Ext.	5.4	A	E
156	S26	28.9895	36.7170	45	79	88	2	187	11	277	0.04	NF	Radial Ext.	11.9	B	E
157	S27	28.9980	36.7100	126	69	73	19	280	9	187	0.2	NF	Radial Ext.	14.6	C	C
158	S28	28.9978	36.7136	54	65	226	24	56	4	325	0.05	NF	Radial Ext.	14.3	C	E
159	S29	29.0169	36.7026	46	77	302	2	40	13	131	0.24	NF	Radial Ext.	5.9	A	E
160	S30	29.0106	36.6936	96	59	250	24	112	19	13	0.36	NF	Pure Ext.	8.9	A	E
161	S31	29.0070	36.6941	96	79	180	2	79	11	349	0.3	NF	Pure Ext.	4.2	A	E
162	S32	29.0111	36.6959	59	48	323	26	86	30	193	0.1	UF	Oblq. Ext.	6.8	A	E
163	S34	29.0793	36.6449	31	77	324	7	203	11	112	0.46	NF	Pure Ext.	2.9	A	E
164	S35	29.0775	36.6458	31	64	343	24	136	10	231	0.57	NF	Pure Ext.	8.6	A	C
165	S36	29.0757	36.6435	109	75	258	15	85	2	354	0.24	NF	Radial Ext.	5.9	A	E
166	S37	29.0369	36.6099	57	43	217	46	49	6	313	0.15	NS	Oblq. TrT.	5.9	A	E
167	S38	29.0501	36.6561	40	88	60	2	248	0	158	0.13	NF	Radial Ext.	5.7	A	E
168	S39	29.0448	36.6548	49	80	209	7	346	7	77	0.01	NF	Radial Ext.	6.4	A	E
169	S40	29.0457	36.6635	80	69	301	12	65	17	159	0.34	NF	Pure Ext.	7.9	A	B
170	S41	29.0418	36.6611	48	89	335	0	97	1	187	0.24	NF	Radial Ext.	14.7	C	E
171	S42	29.0439	36.6570	12	51	35	39	219	2	127	0.78	NS	Oblq. Ext.	8.2	C	E
172	S43	29.0364	36.6676	61	76	40	3	296	13	205	0.34	NF	Pure Ext.	3.6	A	E
173	S44	29.0344	36.6671	38	57	19	32	217	8	122	0.12	NF	Radial Ext.	4.6	A	E
174	S45	29.0306	36.6714	20	52	171	38	352	0	262	0.12	NS	Oblq. Ext.	7.9	B	E
175	S46	29.0881	36.6795	49	39	0	45	216	18	106	0.25	NS	Oblq. TrT.	8.3	A	E
176	S47	29.1083	36.6754	23	58	31	25	252	19	153	0.01	NF	Radial Ext.	11.1	B	E
177	S48	28.9089	36.7132	100	71	310	9	69	16	161	0.14	NF	Radial Ext.	8.5	A	D
178	S49	28.9062	36.7055	28	72	31	6	282	17	190	0.42	NF	Pure Ext.	3.5	A	E
179	S50	28.9010	36.6988	54	82	197	8	33	2	302	0.45	NF	Pure Ext.	4.8	A	E
180	S51	28.8835	36.7008	54	70	326	18	117	9	211	0.22	NF	Radial Ext.	4.8	A	E
181	S52	28.8810	36.7001	54	69	297	21	125	3	34	0.1	NF	Radial Ext.	7.3	A	E
182	S53	28.8676	36.6869	24	64	296	26	108	3	199	0.19	NF	Radial Ext.	3.9	B	E
183	S54	28.8687	36.7089	74	85	290	2	176	5	85	0.22	NF	Radial Ext.	7.7	A	C
184	S55	28.8822	36.7026	77	86	304	2	188	4	98	0.04	NF	Radial Ext.	5.9	A	E
185	S56	28.8662	36.6842	51	85	59	1	311	4	220	0.2	NF	Radial Ext.	10.3	B	E
186	S60	28.8006	36.6752	37	79	190	11	1	2	91	0.41	NF	Pure Ext.	5.9	A	E
187	S61	28.8008	36.6718	116	75	111	8	232	13	323	0.67	NF	Pure Ext.	9.9	B	E
188	S62	28.8073	36.6682	29	88	30	2	193	1	283	0.35	NF	Pure Ext.	7.3	A	D
189	S63	28.7947	36.6586	39	89	194	0	100	1	10	0.08	NF	Radial Ext.	6.3	A	E
190	S64	28.7999	36.6525	27	81	120	9	307	1	216	0.54	NF	Pure Ext.	7.8	A	D
191	S65A	28.8028	36.6559	191	57	287	30	137	14	39	0.15	NF	Radial Ext.	9	A	B
192	S66	28.8037	36.6561	61	80	250	4	4	9	95	0.11	NF	Radial Ext.	4.2	A	C
193	S67	28.8264	36.6523	96	38	343	46	200	19	89	0.52	NS	Oblq. TrT.	5.5	A	E
194	S68	28.9362	36.7190	38	89	134	1	301	0	31	0.04	NF	Radial Ext.	8.5	A	C
195	S69A	28.9378	36.7192	101	88	150	0	244	2	334	0.13	NF	Radial Ext.	7.1	A	C
196	S70	28.9441	36.7080	38	73	294	15	144	8	52	0.21	NF	Radial Ext.	8.3	A	D
197	S71	28.9443	36.7077	79	53	45	36	222	2	313	0.75	NS	Oblq. Ext.	6.1	A	B
198	S72	28.9337	36.6961	145	81	152	1	247	9	337	0.45	NF	Pure Ext.	15.9	D	E
199	S74	28.9297	36.6976	18	65	244	13	3	21	98	0.4	NF	Pure Ext.	11.4	B	E
200	S75	28.9337	36.7008	53	49	131	40	326	7	229	0.44	NS	Oblq. Ext.	6.1	A	B
201	S76	28.9351	36.7066	37	81	8	1	275	9	185	0.34	NF	Pure Ext.	4.9	A	E
202	S77	28.9306	36.7068	36	85	81	5	273	1	183	0.36	NF	Pure Ext.	13	C	C
203	S78	28.9306	36.7093	100	58	351	10	97	30	193	0.03	NF	Radial Ext.	10.8	B	B
204	S79	28.9400	36.7194	27	81	93	7	233	6	324	0.65	NF	Pure Ext.	7.1	A	C
205	S80	28.9421	36.7210	25	72	190	18	6	1	97	0.71	NF	Pure Ext.	10.2	B	B
206	S81	28.9429	36.7228	45	88	103	2	246	1	336	0.21	NF	Radial Ext.	12.9	C	D
207	S82	28.9445	36.7250	31	89	68	1	204	1	294	0.28	NF	Pure Ext.	12	B	B
208	S83	28.9468	36.7253	28	45	208	44	43	7	306	0.33	NS	Oblq. Ext.	5.3	A	E
209	S84	28.8784	36.6438	20	83	98	4	221	6	311	0.13	NF	Radial Ext.	10.6	B	E
210	S85	28.8989	36.6608	57	80	275	3	25	9	115	0.01	NF	Radial Ext.	3.8	A	E
211	S86	28.8935	36.6689	34	63	280	23	135	14	39	0.33	NF	Pure Ext.	5.1	A	E
			Total	**13416**												

D/P: azimuth/Plunge, n: number of samples used for inversion, R stress ratio, QRw and QRt quality estimators, Comp.: Compressive, Ext.: Extensional, Oblq: oblique, St.S.: Strike-slip, TrT.: Transtensive.

or location. However, they generally tend to develop close to normal fault terminations and relay areas. Therefore, they are interpreted as accommodation structures that transfer the differential extensional deformation between two or more normal faults. Similarly, lack of any major strike-slip fault and related deformational structures such as the absence of any flower structures pertinent to strike-slip faults on the seismic sections challenges the presence of a regional strike-slip fault zone in the region as was proposed previously. In other words, the study

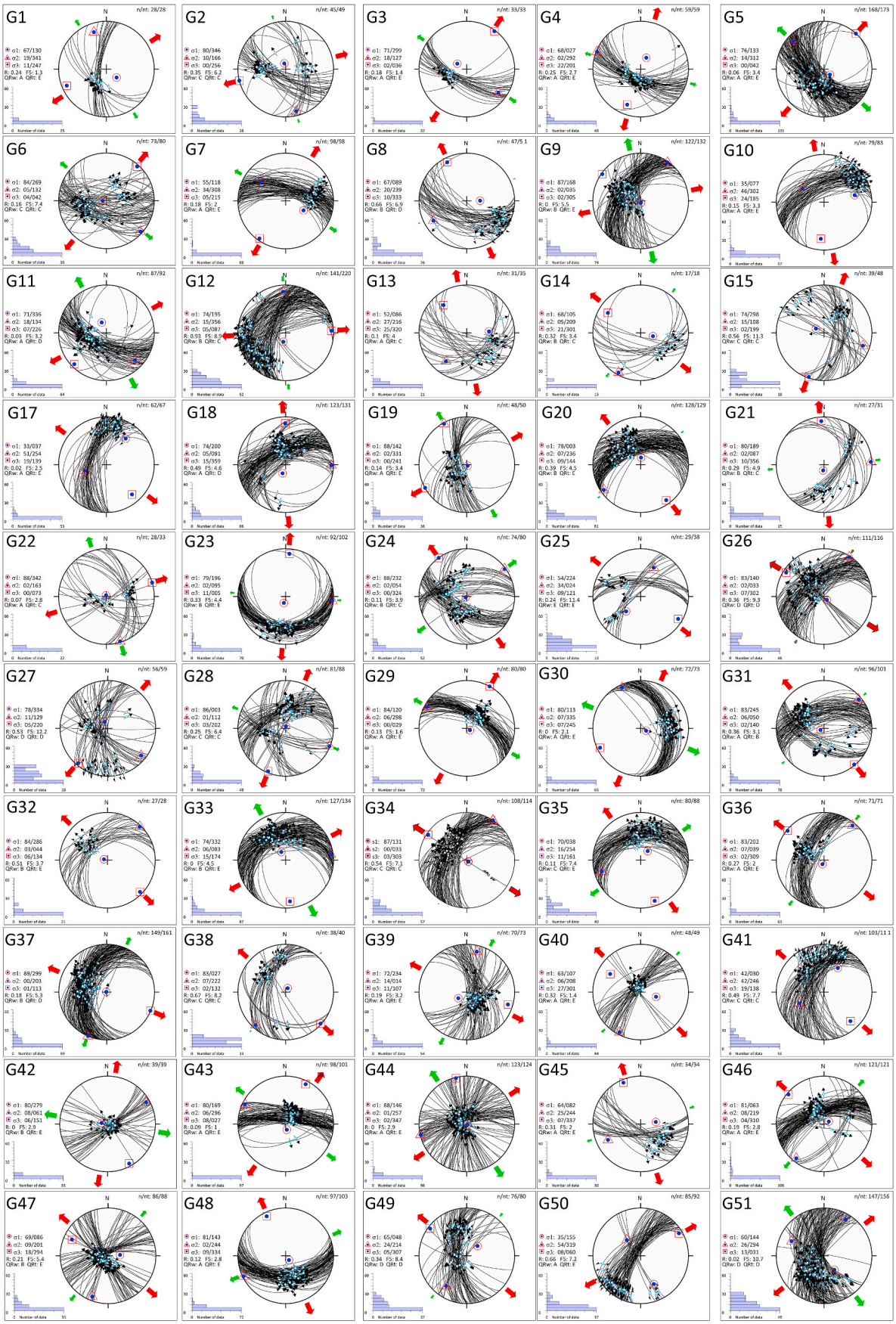

Fig. 9. Cyclographic traces and orientations of constructed paleostress configurations for each site. See Table 2 for the details of each site and the meanings of each abbreviation.

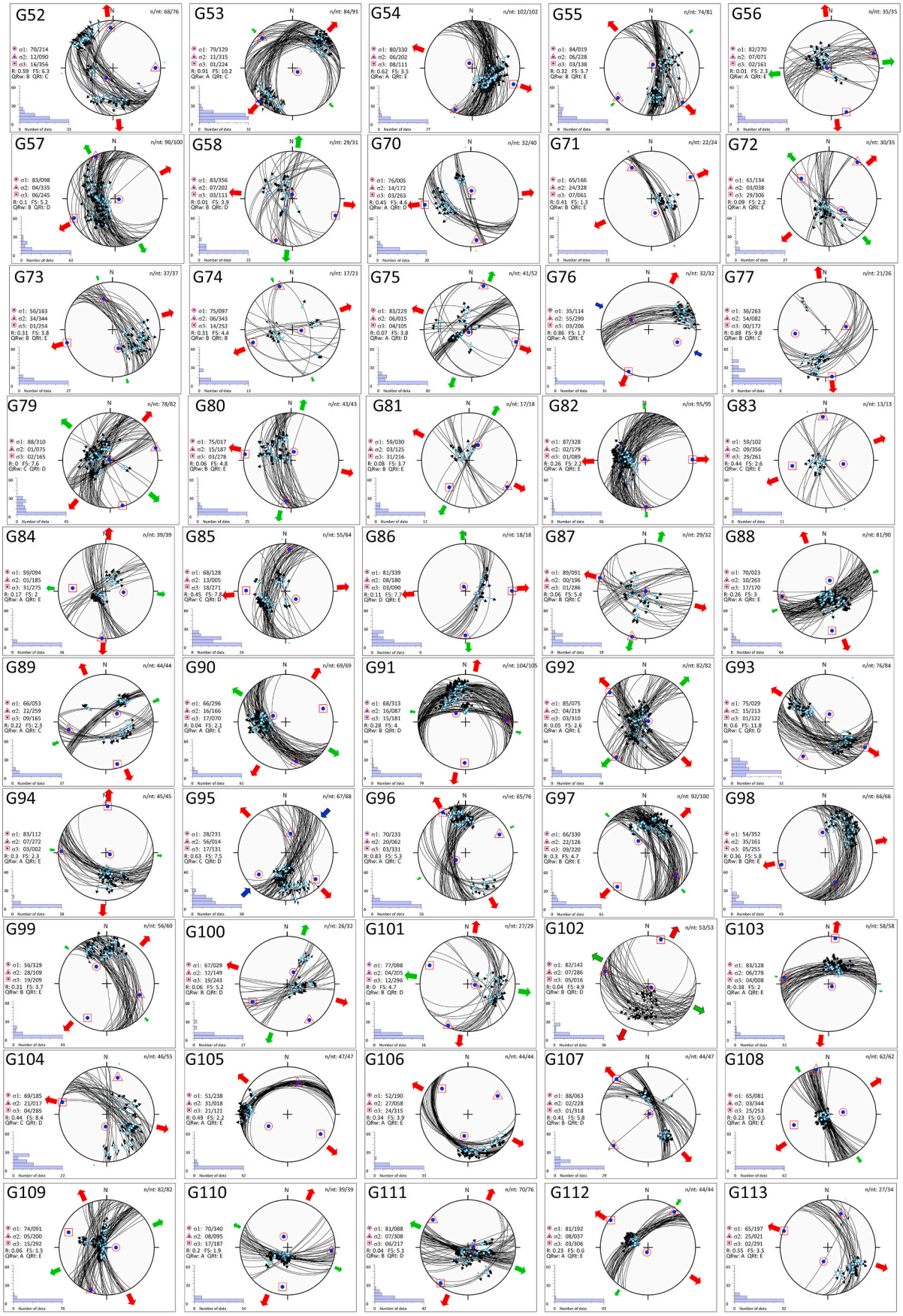

Fig. 9. (*continued*).

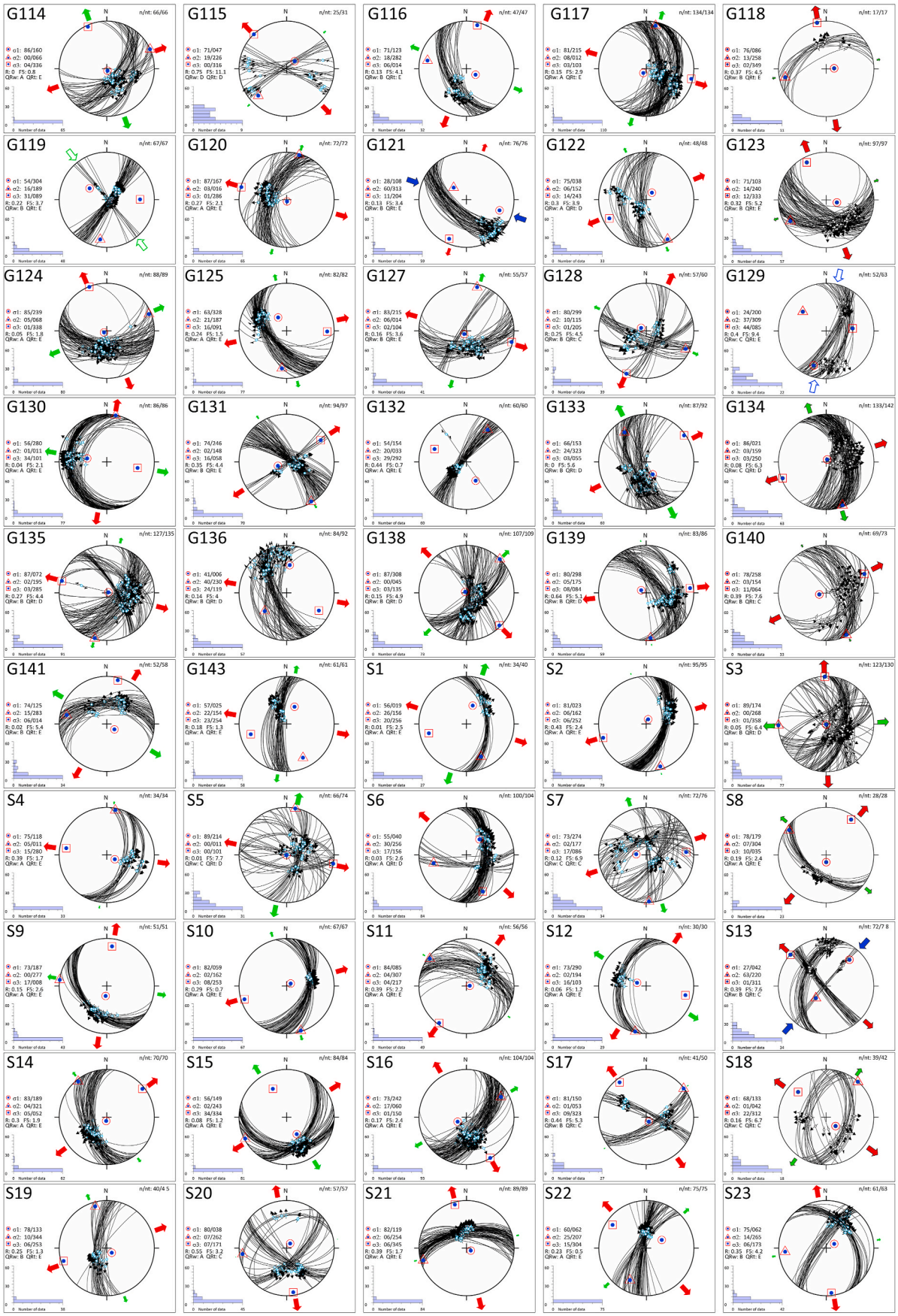

Fig. 9. (*continued*).

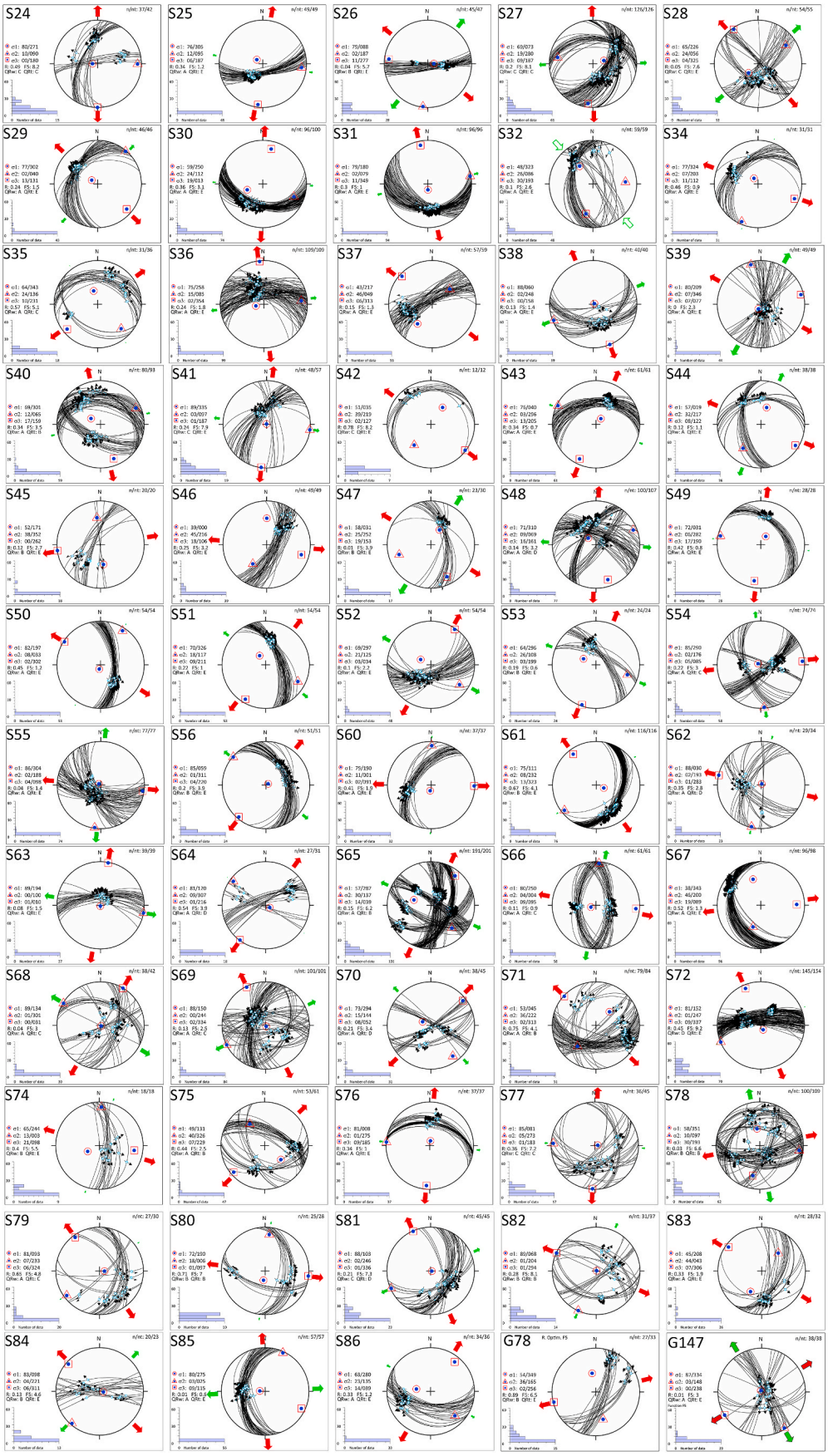

Fig. 9. (*continued*).

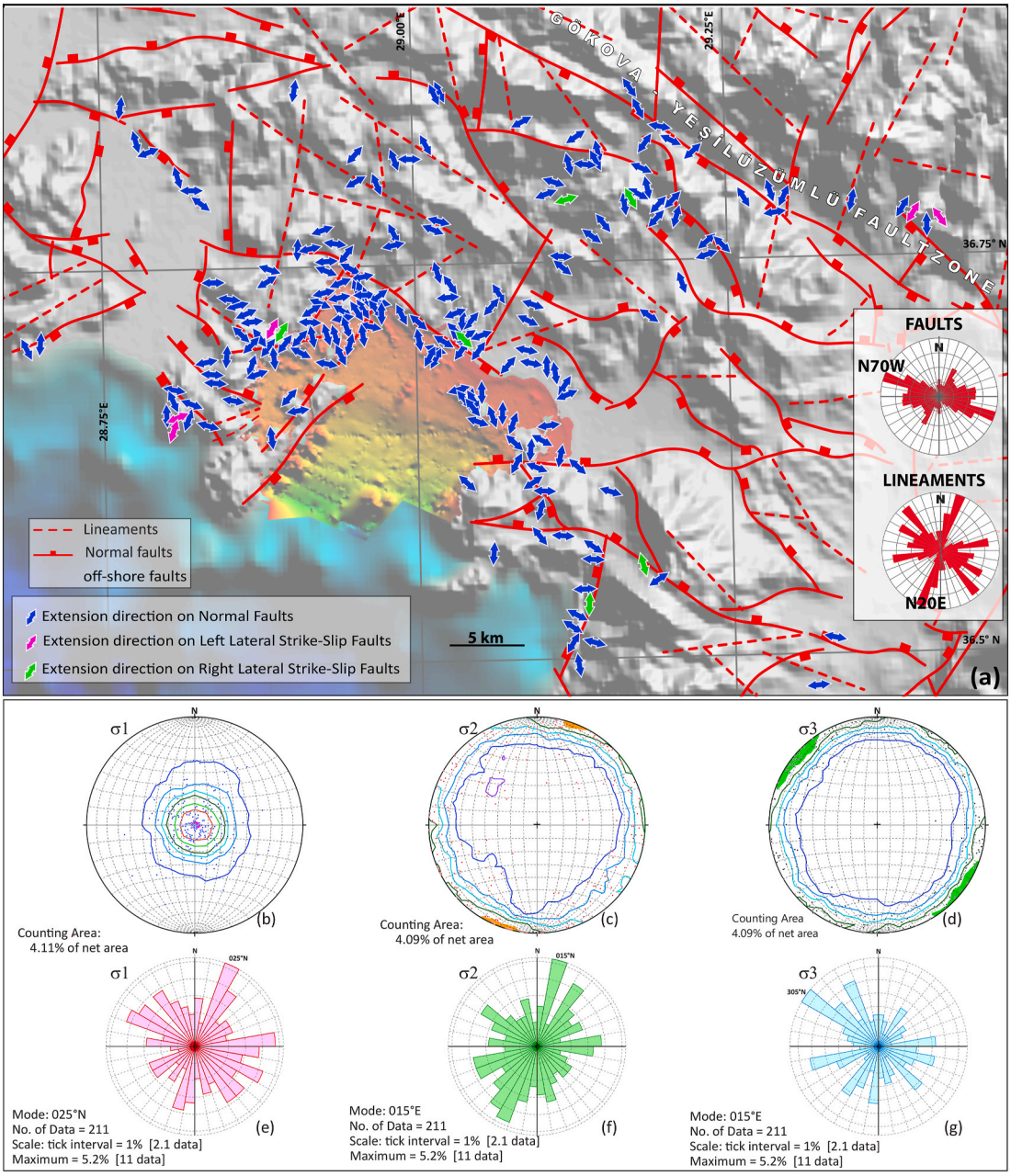

Fig. 10. a) Structural map of the study area and horizontal projection of minor stress orientations per site (See Table 2 and Fig. 9 for paleostress configuration of each site). Contour diagrams of principal stress orientations (b–d), and rose diagrams of their horizontal components (e–f). Note near-vertical, but the scattered distribution of σ_1 (a) and near-horizontal but almost uniformly scattered distributions of σ_2 and σ_3 axes (b&c).

area lacks any major regional strike-slip fault zone but is dominated by multi-directional extension and related normal and their transfer faults.

Based on the interpretation of multibeam data, Ocakoğlu (2012) proposed that several faults with apparent lateral offsets were located a few tens of kilometers off-shore areas. Moment tensor solutions of recent earthquakes indicate the presence of strike-slip faults a few kilometers south of the study area (Fig. 3). However, on-shore moment tensor solutions indicate only normal faulting, strike-slip faulting related earthquakes are lacking on-land areas. Having strike-slip moment tensor solutions, and mapped strike-slip faults (Ocakoğlu, 2012) in the deeper parts of the Fethiye-Göcek Bay together with lack of earthquakes with strike-slip moment tensor solutions and lack of paleostress configurations with strike-slip deformation on-land areas collectively indicate that the strike-slip faulting terminates very close to the shoreline around Fethiye-Göcek Bay. In other words, it seems that the Pliny-Strabo Trench does not propagate northwards into the SW Anatolian continental areas (Fig. 14).

Most of the off-shore earthquakes with sinistral strike-slip components may be related to the tearing of the northern edge of the subducted African Oceanic lithosphere (Fig. 14), which resulted in the development of Pliny-Strabo Trench. However, lack of earthquakes with strike-slip moment tensor solutions and lack of any major faults with strike-slip character on-land areas indicate that the strike-slip faults have not propagated on-land areas. This implies that the Pliny-Strabo Trench is a typical trench-trench connecting transform fault, a structure extending from the SE corner of South Aegean trench up to the northern margin of Rhodes Basin and connecting the South Aegean and Cyprian trenches (Özbakır et al., 2013, 2017; Bocchini et al., 2018; Kaymakcı et al., 2018; Ganas et al., 2018).

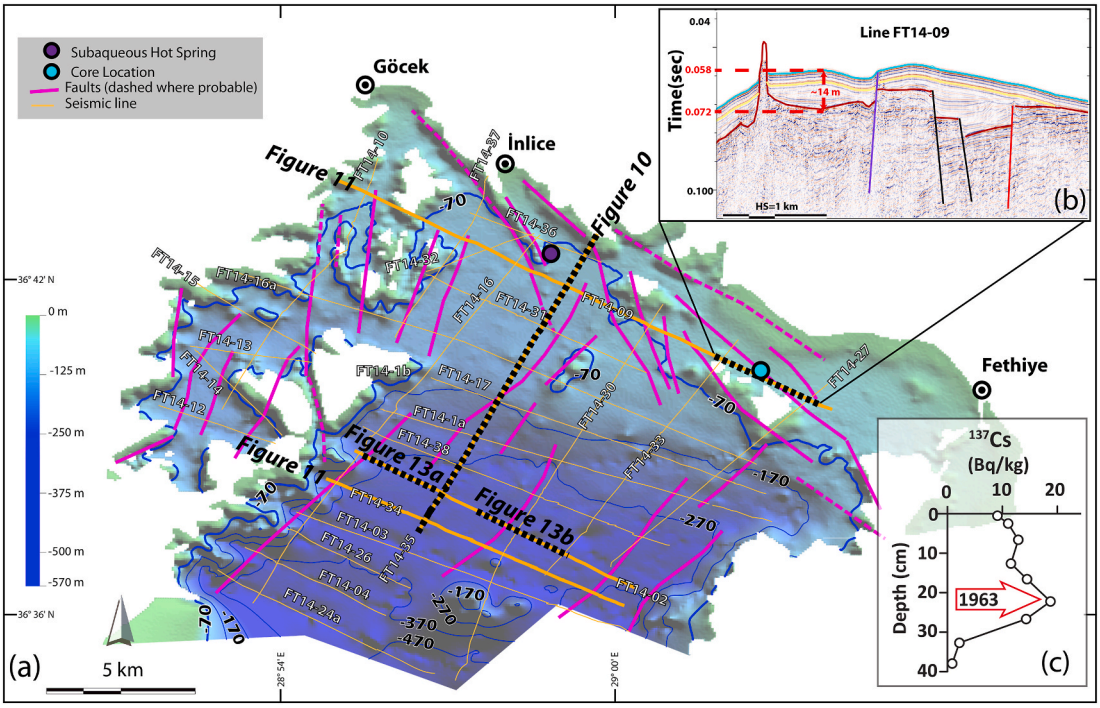

Fig. 11. a) position of 2D Seismic lines overlaid on colour coded bathymetry. 70 m contour which is thought to be paleo shoreline (Hall et al., 2014) is highlighted, and location of subaqueous hot spring and the gravity core location as b) Active faults on seismic line FT14-09 and Near Base of the Holocene is picked by a red line. c) 137Cs plot for the top 40 cm of the sediment core. The peak in 1963 due to atmospheric nuclear weapon tests is located around 21 cm depth. (For interpretation of the references to color in this figure legend, the reader is referred to the Web version of this article.)

6.1. Regional implications

In SW Anatolia, a sinistral transtensional fault/shear zone has been proposed as the on-land continuation of Pliny-Strabo Trenches (PST) on the basis of the concept of STEP fault (c.f. Govers and Wortel 2005), the so-called Fethiye Burdur Fault (or Shear) Zone (FBFZ). By definition, STEP faults are large-scale shear zones where the subducting lithosphere is laterally decoupled from non-subducting lithosphere in a scissor-type of fashion. Therefore, they display similar deformation patterns to strike-slip faults characterized by an array of subsidiary brittle fractures (e.g. Riedel and P shears). Moreover, depending on the tectonic setting, the type of deformation occurring in STEP fault zones can vary from transpression to transtension. In this context, following the recognition of a tear on the subducting and retreating African lithosphere based on tomographic studies (Govers and Wortel 2005), further subsurface studies (e.g. van Hinsbergen et al., 2010; Biryol et al., 2011) revealed that the Pliny-Strabo Trench is a transpressional STEP fault connecting the Aegean and Cyprian trenches along the northern edge of the northwards subducting African lithosphere (see Özbakır et al., 2013 ful account of the structure). Based on the collinearity between Pliny-Strabo Trench and the NE-SW trending faults extending from Fethiye to Burdur, it was proposed that FBFZ is a sinistral strike-slip fault zone and the NE propagation of Pliny-Strabo Trench into the SW Anatolia (Hall et al., 2014). However, the proposed trench propagation model of FBFZ has not been verified by field data. On the other hand, recent studies based on GNSS observations indicate that the SW Turkey is extending both N–S, NNW-SSE and NE-SW directions which kinematically invalidates the need for an on-shore strike-slip fault zone (Howell et al., 2017; Ganas et al., 2018). Based on the distribution and depths of recent seismic activity, Boccini et al. (2018) proposed two different slab tears in the subducted African oceanic slab in the region. One of them is oriented in an NW-SE direction almost parallel to the Turkish shoreline while the second one is oriented NE-SW, parallel to Pliny-Strabo Trenches but located further east. A recent paleomagnetic (Kaymakci et al., 2018) study conducted in SW Anatolia argued that there is no marked differential rotation within and either side of the proposed FBFZ. Similarly, Özkaptan et al. (2021) concurred that the strain pattern in SW Anatolia is gradually changing from Beydağları in the east to the Aegean Sea in the west, and there is no abrupt change along the proposed FBFZ. They suggested that such a major strike-slip fault zone would have produced an abrupt change in the rotation and strain pattern.

Consequently, the overall kinematics of faults, fault plane solutions of earthquakes, and subsurface data throughout the study area indicate that the study area is under the control of multi-directional extension dominated by WNW-ESE directed extension, and almost all of the faults in the study area are normal in character. Therefore they do not support the presence of a NE-SW striking strike-slip shear zone in the study area and therefore confute the idea of north-eastward propagation of PST into SW Anatolia. These data, together with recent paleomagnetic, GNSS velocity, and seismotectonic studies in the region, indicate that the sinistral strike-slip deformation associated with Pliny-Strabo Trenches terminates very close to the shoreline in the Fethiye-Göcek Bay area. In other words, the Pliny-Strabo Trenches do not propagate into the on-land areas.

7. Conclusions

Fault orientations and their activities allowed the deformation styles around Fethiye-Göcek Bay to be unravelled. Using Angelier's reduced stress tensor procedure, the paleostress configurations and their relative magnitudes (i.e., the shape of stress ellipsoid) were deduced from fault slip data set collected in the field. The seismic interpretation studies provided region-wide traceable horizons and facilitated the interpretation of active faults in the bay. The off-shore and on-shore faults are correlated through the study area. The paleostress configurations proved that the region has been deforming under multi-directional extension with slight domination of NW-SE directed extensional deformation, manifested by predominantly NE-SW striking active normal faults. Apart from those faults, few NW-SE trending strike-slip faults were identified. They are developed almost perpendicular to NE-SW trending normal

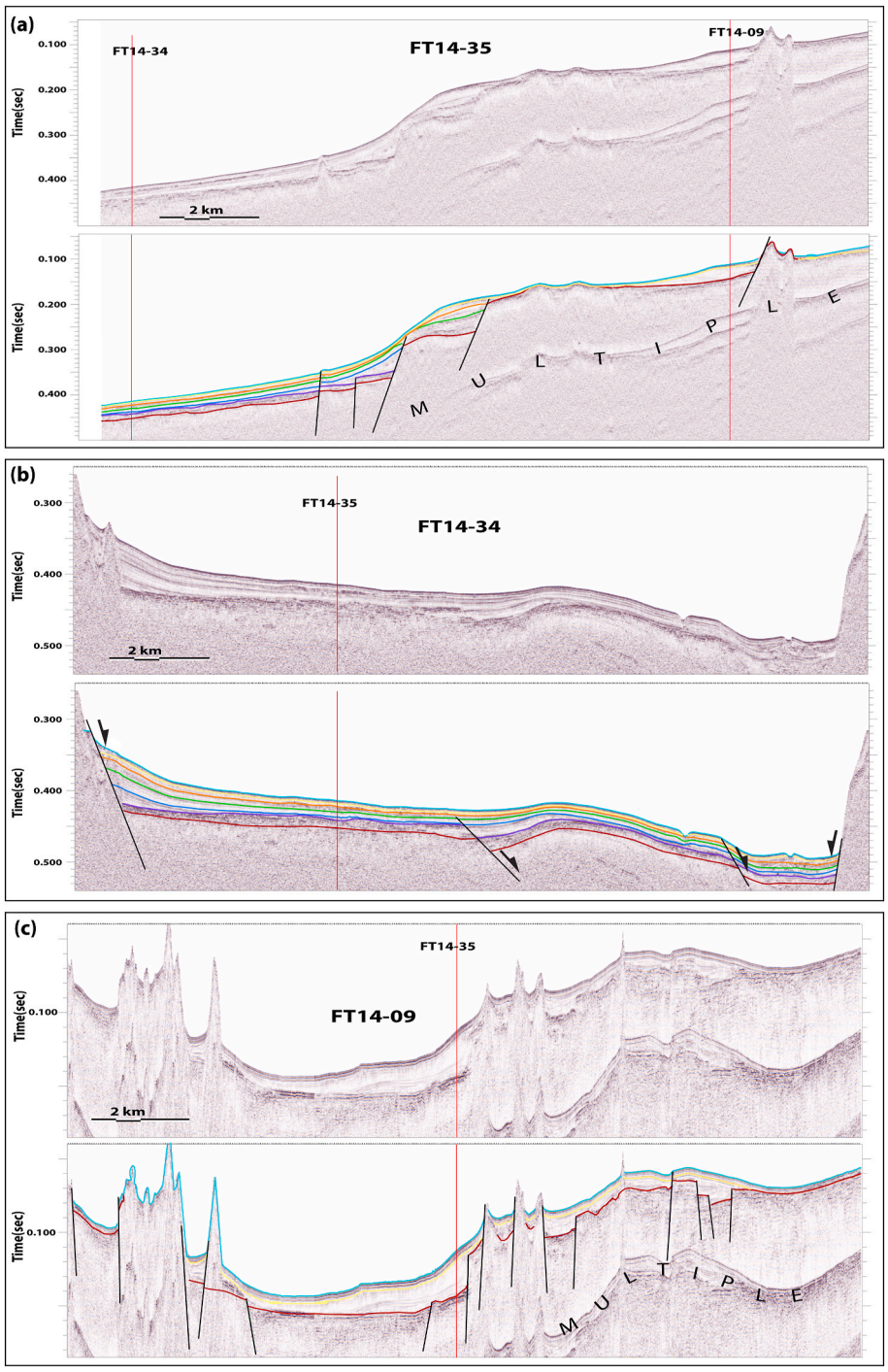

Fig. 12. Picked horizons and the interpreted faults on various seismic lines. See Fig. 11 for their locations.

faults and are interpreted to be transfer faults that accommodate differential displacement between two adjacent segments of the normal faults. Almost all these normal faults are developed around the Fethiye-Göcek Bay located at the north-eastern termination of the Pliny-Strabo Trench.

Based on the literature data, recent seismic activity, fault kinematics, and interpretation of shallow seismic reflection data from Fethiye-Göcek Bay, the following conclusions are reached;

1. Recent earthquake activity indicates normal faulting of on-land areas and strike-slip faulting off-shore.
2. The region has been deforming under the influence of multi-directional extensional deformation manifested by normal faults with high angle pitches of slickensides on the fault planes.
3. Several approximately N–S to NE-SW striking faults are encountered in the Fethiye-Göcek Bay. Most of these faults cut and displace the sea bed and are interpreted as the evidence for the activity of the normal faulting in the region.
4. Our results indicate that the strike-slip faulting related to Pliny-Strabo Trenches terminates very close to the shoreline but does not propagate into the on-land areas. Therefore, they do not support the possibility that the Pliny-Strabo Trench extends on-land as a sinistral strike-slip fault.

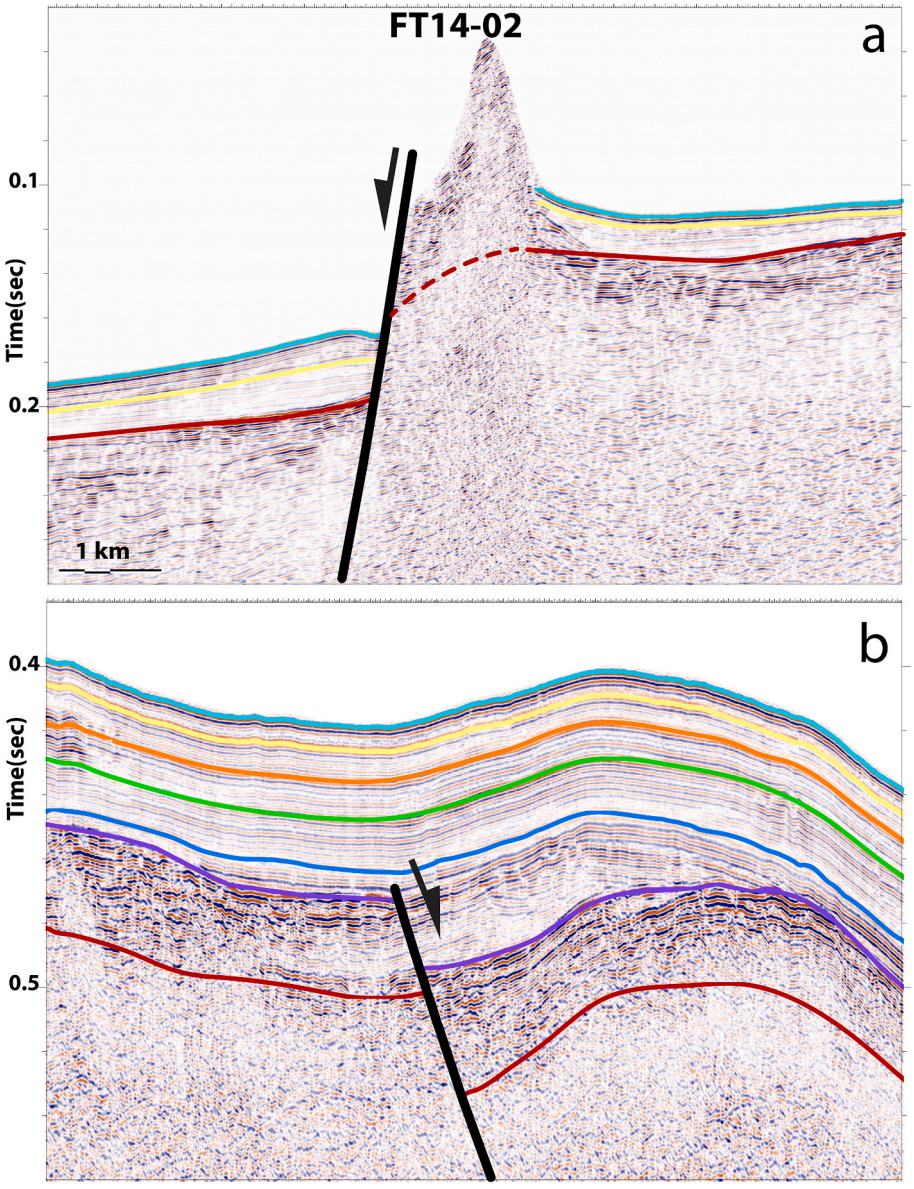

Fig. 13. Seismic facies characteristics used for interpretation of faults.

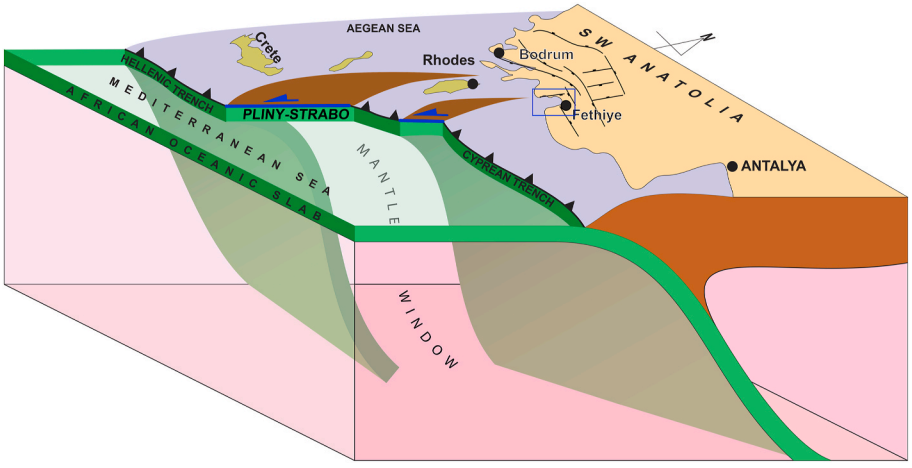

Fig. 14. A conceptual block diagram illustrating the development of a series of tear along the Pliny-Strabo Trench. Note that the tear has not propagated into the on-land areas in SW Anatolia nor Fethiye-Göcek Bay (indicated with box). On-land normal faults are simplified.

Credit author statement

Levent Tosun: Methodology, investigation, formal analysis, software, writing. **Ulaş Avşar**: Project administration, investigation, validation, writing-review. **Özgür Avşar**: funding acquisition, formal analysis, validation, writing-review. Derman Dondurur: Resources, data curation. Nuretdin Kaymakci: Conceptualization, methodology, validation, formal analysis, resources, funding acquisition, supervision, writing-review.

Declaration of competing interest

The authors declare that they have no known competing financial interests or personal relationships that could have appeared to influence the work reported in this paper.

Acknowledgements

The seismic reflection data interpreted in this study were collected for a project supported by the Scientific and Technological Research Council of Turkey (TÜBİTAK) (Grand Number 112Y137). Field studies are supported by a Tubitak Project (Grant Number 111Y239). 137Cs measurements are supported by King Abdullah University of Science and Technology (KAUST). We would like to thank Professor Thomas Blenkinsop of Cardiff university for improving the English of the text. We thank M. Cihat Alçiçek and an anonymous reviewer for their constructive criticisms.

Appendix A. Supplementary data

Supplementary data to this article can be found online at https://doi.org/10.1016/j.jsg.2021.104287.

References

AFAD, 2019. Disaster and Emergency Management Authority, Earthquake Department Catalogue, pp. 1900–2019. http://www.deprem.gov.tr/sarbis/Veritabani/DDA.aspx?param=1.

Alçiçek, M.C., Ten Veen, J.H., Özkul, M., 2006. Neotectonic development of the Çameli basin, south-western Anatolia, Turkey. Geol. Soc.London 260 (1), 591–611. Special Publ.

Alçiçek, M.C., 2007. Tectonic development of an orogen-top rift recorded by its terrestrial sedimentation pattern: the Neogene Eşen Basin of south-western Anatolia, Turkey. Sediment. Geol. 1 (200), 117–140.

Alçiçek, M.C., ten Veen, J.H., 2008. The late Early Miocene Acipayam piggy-back basin: refining the last stages of Lycian nappe emplacement in SW Turkey. Sediment. Geol. 208, 101–113.

Alçiçek, M.C., Brogi, A., Capezzuoli, E., Liotta, D., Meccheri, M., 2013. Superimposed basin formation during Neogene–Quaternary extensional tectonics in SW-Anatolia (Turkey): insights from the kinematics of the Dinar Fault Zone. Tectonophysics 608, 713–727.

Allmendinger, R.W., Siron, C.R., Scott, C.P., 2017. Structural data collection with mobile devices: accuracy, redundancy, and best practices. J. Struct. Geol. 102, 98–112.

Avşar, Ö., Avşar, U., Arslan, Ş., Kurtuluş, B., Niedermann, S., Güleç, N., 2017. Subaqueous hot springs in köyceğiz lake, dalyan channel and Fethiye-Göcek bay (SW Turkey): locations, chemistry and origins. J. Volcanol. Geoth. Res. 345, 81–97.

Angelier, J., 1994. Fault slip analysis and paleostress reconstruction. Continental deformation 53–101.

Barka, A., Reilinger, R., 1997. Active tectonics of the Eastern Mediterranean region: deduced from GPS, neotectonic and seismicity data. Ann. Geophys. 40 (3), 587–610.

Biryol, C.B., Beck, S.L., Zandt, G., Özacar, A.A., 2011. Segmented African lithosphere beneath the Anatolian region inferred from teleseismic P-wave tomography. Geophys. J. Int. 184 (3), 1037–1057.

Blumenthal, M.M., 1963. Le système structural du Taurus sud Anatolies. Bill. Soc. Géol. Fr. In: Livre à Mémoire de Professor P. Fallot. Mem. Soc. Geol. Fr. 1 (2), 611–662.

Bocchini, G.M., Brüstle, A., Becker, D., Meier, T., van Keken, P.E., Ruscic, M., Papadopoulos, G.A., Rische, M., Friederich, W., 2018. Tearing, segmentation, and backstepping of subduction in the Aegean: new insights from seismicity. Tectonophysics 734, 96–118.

Bozkurt, E., Park, R.G., 1994. Southern Menderes Massif: an incipient metamorphic core complex in western Anatolia, Turkey. London J. Geol. Soc. 151, 213–216.

Collins, A.S., Robertson, A.H., 1997. Lycian melange, south-western Turkey: an emplaced Late Cretaceous accretionary complex. Geology 25 (3), 255–258.

Delvaux, D., Sperner, B., 2003. Stress tensor inversion from fault kinematic indicators and focal mechanism data: the TENSOR program. New insights .Struct. Interpretation.Model 212, 75–100.

Dumont, J.F., Uysal, Ş., Şimşek, Ş., Karamanderesi, I.H., ve Letouzey, J., 1979. Güneybatı anadolu'daki Grabenlerin Oluşumu. Maden Tetkik ve Arama Dergisi 97, 7–17 (In Turkish).

Elitez, İ., 2010. The Miocene-Quaternary Geodynamics of Çameli and Gölhisar Basins, Burdur-Fethiye Fault Zone. Istanbul Technical University, unpublished MSc Thesis.

Eyidoğan, H., Barka, A., 1996. The 1 October 1995 dinar earthquake, SW Turkey. Terra. Nova 8 (5), 479–485.

Ganas, A., Pavlides, S., Karastathis, V., 2005. DEM-based morphometry of range-front escarpments in Attica, central Greece, and its relation to fault slip rates. Geomorphology 65 (3–4), 301–319.

Ganas, A., Elias, P., Kapetanidis, V., Valkaniotis, S., Briole, P., Kassaras, I., et al., 2018. The july 20, 2017 M6. 6 kos earthquake: seismic and Geodetic evidence for an active north-dipping normal fault at the western end of the Gulf of Gökova (SE Aegean Sea). Pure Appl. Geophys. 1–35.

Govers, R., Wortel, M.J.R., 2005. Lithosphere tearing at STEP faults: response to edges of subduction zones. Earth Planet Sci. Lett. 236 (1–2), 505–523.

Hall, J., Aksu, A.E., Elitez, I., Yaltırak, C., Çifçi, G., 2014. The Fethiye-Burdur Fault Zone: a component of upper plate extension of the subduction transform edge propagator fault linking Hellenic and Cyprus Arcs, Eastern Mediterranean. Tectonophysics 635, 80–99.

Hayward, A.B., 1984. Miocene clastic sedimentation related to the emplacement of the Lycian Nappes and the antalya complex, SW. Turkey. In: Dixon, J.E., Robertson, A.H.F. (Eds.), The Geological Evolution of the Eastern Mediterranean, vol. 17. Geol. Soc. London, Spec. Publ., pp. 287–300

Howell, A., Jackson, J., Copley, A., McKenzie, D., Nissen, E., 2017. Subduction and vertical coastal motions in the eastern Mediterranean. Geophys. J. Int. 211 (1), 593–620. https://doi.org/10.1093/gji/ggx307.

Kaymakcı, N., Langereis, C., Özkaptan, M., Özacar, A.A., Gülyüz, E., Uzel, B., Sözbilir, H., 2018. Paleomagnetic evidence for upper plate response to a STEP fault, SW Anatolia. Earth Planet Sci. Lett. 498, 101–115.

Kaymakçı, N., Özacar, A., Özkaptan, M., Koç, A., Gülyüz, E., Lefebvre, C., Sözbilir, H., 2014. Fethiye-Burdur fault zone: a myth. In: The 8th International Symposium on Eastern Mediterranean Geology (ISEMG-8) (13-17).

Kaymakci, N., Özçelik, Y., White, S.H., Van Dijk, P.M., 2009. Tectono-stratigraphy of the Çankırı Basin: late Cretaceous to early Miocene evolution of the Neotethyan suture zone in Turkey. Geol. Soc.London 311 (1), 67–106. Special Publ.

Kiratzi, A., Aktar, M., Svigkas, N., 2013. Bulletin of the geological Society of Greece. In: Proceedings of the 13th International Congress, Chania, 5-8 September 2013, XLVII 2013.

Koçyiğit, A., Saraç, G., 2000. Episodic graben formation and extensional neotectonic regime in west Central Anatolia and the Isparta Angle: a case study in the Akşehir-Afyon Graben, Turkey. Geol. Soc.London 173 (1), 405–421. Special Publ.

Le Pichon, X., Angelier, J., 1979. The Hellenic arc and trench system: a key to the neotectonic evolution of the eastern Mediterranean area. Tectonophysics 60 (1), 1–42.

Lee, S., Suh, J., Park, H.D., 2013. Smart Compass-Clinometer: a smartphone application for easy and rapid geological site investigation. Comput. Geosci. 61, 32–42.

Machette, M.N., 2000. Active, capable, and potentially active faults—a paleoseismic perspective. J. Geodyn. 29 (3–5), 387–392.

McKenzie, D., 1978. Active tectonics of the alpine—himalayan belt: the Aegean Sea and surrounding regions. Geophys. J. Int. 55 (1), 217–254.

MTA, 2002. Geological Map of Turkey, 1/500,000 Scaled Zonguldak Quadrangle. MTA Genel Mudurlugu, Ankara, Turkey.

Novakova, L., Pavlis, T.L., 2017. Assessment of the precision of smart phones and tablets for measurement of planar orientations: a case study. J. Struct. Geol. 97, 93–103.

Ocakoğlu, N., 2012. Investigation of Fethiye-marmaris bay (SW Anatolia): seismic and morphologic evidences from the missing link between the Pliny Trench and the Fethiye-Burdur Fault zone. Geo Mar. Lett. 32 (1), 17–28.

Okay, A.I., 2001. Stratigraphic and metamorphic inversions in the central Menderes Massif: a new structural model. Int. J. Earth Sci. 89 (4), 709–727.

O'leary, D.W., Friedman, J.D., Pohn, H.A., 1976. Lineament, linear, lineation: some proposed new standards for old terms. Geol. Soc. Am. Bull. 87 (10), 1463–1469.

Özbakır, A.D., Govers, R., Wortel, R., 2017. Active faults in the Anatolian-Aegean plate boundary region with Nubia. Turk. J. Earth Sci. 26 (1).

Özbakır, A.D., Şengör, A.M.C., Wortel, M.J.R., Govers, R., 2013. The Pliny-Strabo trench region: a large shear zone resulting from slab tearing. Earth Planet Sci. Lett. 375, 188–195.

Özer, S., Sözbilir, H., Özkar, Ý., Toker, V., Sarı, B., 2001. Stratigraphy of upper Cretaceous- palaeogene sequences in the southern and eastern Menderes Massif (western Turkey). Int. J. Earth Sci. 852–866.

Özgül, N., 1984. Stratigraphy and tectonic evolution of the central Taurides (Ankara). In: Tekeli, O., Goncuoglu, M.C. (Eds.), Geology of the Taurus Belt, pp. 77–90.

Özkaptan, M., Kaymakcı, N., Langereis, C.G., Gülyüz, E., Arda Özacar, A., Uzel, B., Sözbilir, H., 2018. Age and kinematics of the Burdur basin: Inferences for the existence of the Fethiye Burdur Fault zone in SW Anatolia (Turkey). Tectonophysics 744, 256.

Özkaptan, M., Gülyüz, Uzel, B.E., Langereis, C.G., Arda Özacar, A., Kaymakcı, N., 2021. Revealing the deformation of SW Anatolia (Turkey) by anisotropy of magnetic Susceptibility (AMS) data. Tectonics (In Review). https://doi.org/10.1002/essoar.10503026.1.

Poisson, A., 1984. The extension of the Ionian trough into south-western Turkey. Geol. Soc.London.Special Publ. 17 (1), 241–249.

Poisson, A., Yağmurlu, F., Bozcu, M., Şentürk, M., 2003. New insights on the tectonic setting and evolution around the apex of the Isparta Angle (SW Turkey). Geol. J. 38 (3-4), 257–282.
Şengör, A.M.C., Yilmaz, Y., 1981. Tethyan evolution of Turkey: a plate tectonic approach. Tectonophysics 75 (3–4), 181193203–190199241.
Sharma, P.V., 1997. Environmental and Engineering Geophysics. Cambridge university press.
Shebalin, N.V., Karnik, V., Hadzievski, D., 1974. Catalogue of earthquakes of the Balkan region, I, UNDP-UNESCO Survey of the seismicity of the Balkan region. Skopje 600p.
Simón, J.L., 2019. Forty years of paleostress analysis: has it attained maturity? J. Struct. Geol. 125, 124–133.
Tan, O., Tapirdamaz, M.C., Yörük, A., 2008. The earthquake catalogues for Turkey. Turk. J. Earth Sci. 17 (2), 405–418.
Taymaz, T., Jackson, J., McKenzie, D., 1991. Active tectonics of the north and central Aegean Sea. Geophys. J. Int. 106 (2), 433–490.
Taymaz, T., Price, S., 1992. The 1971 May 12 Burdur earthquake sequence, SW Turkey: a synthesis of seismological and geological observations. Geophys. J. Int. 108 (2), 589–603.
ten Veen, J.H., Boulton, S.J., Alçiçek, M.C., 2009. From palaeotectonics to neotectonics in the Neotethys realm: the importance of kinematic decoupling and inherited structural grain in SW Anatolia (Turkey). Tectonophysics 1 (473), 261–281.
Tiryakioğlu, İ., Floyd, M., Erdoğan, S., Gülal, E., Ergintav, S., McClusky, S., Reilinger, R., 2013. GPS constraints on active deformation in the Isparta Angle region of SW Turkey. Geophys. J. Int. 195 (3), 1455–1463.
van Hinsbergen, D.J., Kaymakci, N., Spakman, W., Torsvik, T.H., 2010. Reconciling the geological history of western Turkey with plate circuits and mantle tomography. Earth Planet Sci. Lett. 297 (3–4), 674–686.
Woodside, J.M., Mascle, J., Zitter, T.A.C., Limonov, A.F., Ergün, M., Volkonskaia, A., 2002. The Florence rise, the western bend of the Cyprus arc. Mar. Geol. 185 (3), 177–194.